Defence recognition of a stripe rust fungal effector is uncoupled from disease outcomes in wheat

Eric C. Pereira[1]╬, Bayantes Dagvadorj[1]╬, Rita Tam[1], Haoran Li[1], Danish Ilyas Baig[1], Mareike Möller[1], Miraclemario Raphael[1], Simon Williams[1], Sambasivam Periyannan[1,2,3], Florence Danila[1], John P. Rathjen[1], and Benjamin Schwessinger[1]

[1]Research School of Biology, The Australian National University, Canberra, ACT, 2601 Australia

[2]Commonwealth Scientific and Industrial Research Organisation Agriculture and Food, Canberra ACT 2601, Australia

[3]School of Agriculture and Environmental Science, Centre for Crop Health, University of Southern Queensland, Toowoomba, QLD 4350, Australia

╬ shared co-first authors

***Corresponding author:** *benjamin.schwessinger@anu.edu.au*

Abstract

Plant resistance (*R*) and pathogen avirulence (*Avr*) gene interactions are central to pathogen recognition and disease resistance in crops. Functional characterisation of recognised *Avr* effectors of *Puccinia striiformis* f. sp. *tritici* (*Pst*) lags other key fungal pathogens of wheat. Here, we used a wheat protoplast-based screen to identify *Avr*/*R* interactions via the proxy of effector-induced defence responses in a set of diverse wheat cultivars. We identified an *Avr* candidate, termed *AvrPstB48,* that triggers

defence responses in 16 out of 24 cultivars tested. *AvrPstB48* is hemizygous, and the *Pst* genome carries four divergent paralogs within a gene cluster. Analysis of these paralogs revealed partial redundancy in their ability to activate wheat defences and enabled us to identify a single amino acid in *AvrPstB4*8 that is necessary but not sufficient for defence activation. Notably, the activation of defence signalling by *AvrPstB48* in protoplasts did not directly correlate with disease outcomes. Whole-plant infection assays revealed that some cultivars which exhibited strong defence activation in the protoplast assay are susceptible to the *Pst* isolate Pst104E137A- from which *AvrPstB48* is derived. Comparison of infection dynamics of two wheat cultivars that differ in their *AvrPstB48* recognition capacity revealed a delay in disease progression in the recognising cultivar Avocet *S* compared to the non-recognising cultivar Morocco. While correlative only, our observations, combined with other recent reports, support a 'recognize-then-suppress' model of plant-pathogen interaction where disease outcomes are driven not only by simple *Avr/R* interactions but also by pathogen effectors that suppress defence signalling downstream of effector recognition.

Keywords: *Puccinia striiformis* f. sp. *tritici*, effectors, avirulence genes, protoplast screening, wheat resistance, plant defence.

INTRODUCTION

Plant pathogenic fungi are major threats to crop yields globally. This is exemplified by wheat stripe (yellow) rust caused by *Puccinia striiformis* f. sp. *tritici* (*Pst*), which causes significant crop losses driven by the ongoing intercontinental spread and rapid host

47 adaptation of this fungus (Hovmøller et al., 2010; 2025). On the molecular level,
48 disease is caused by a large set of effector proteins that are secreted during wheat
49 (Wang et al., 2023). These effectors modulate host cellular processes to facilitate host
50 colonisation, including nutrient acquisition and suppression of defence responses
51 (Zheng et al., 2023). The suppression of defence responses is especially important for
52 biotrophic plant pathogens such as *Pst* which require living host tissue for prolonged
53 periods to complete their lifecycles (Schwessinger, 2017). A subset of effectors
54 designated avirulence (*Avr*) effectors are detected by host resistance (*R*) genes in
55 certain genotypes and cultivars (Xia et al., 2020). *Avr* recognition triggers a myriad of
56 defence responses that restrict pathogen colonisation, including transcriptional
57 reprogramming and, at times, programmed cell death (Dodds & Rathjen, 2010).
58 Several *Avr* genes from other wheat rust fungi have been cloned including *AvrSr13,*
59 *AvrSr22, AvrSr27, AvrSr35, AvrSr50*, and *AvrSr62* from *P. graminis* f. sp. *tritici* (Arndell
60 et al., 2024; Chen et al., 2017; Chen et al., 2024; Outram et al., 2024; Upadhyaya et
61 al., 2021; Salcedo et al., 2017) and *AvrLr15* and *AvrLr21* from *P. triticina* (Cui et al.,
62 2024; Shen et al., 2024). Similar advances have been reported for *Blumeria graminis*,
63 with the identification of *AvrPm2* (Praz et al., 2017) and *AvrPm3* (Bourras et al., 2019),
64 and *Zymoseptoria tritici* with the identification of *AvrStb6*, *Avr3D1* and *AvrStb9*
65 (Amezrou et al., 2023; Meile et al., 2018; Zhong et al., 2017).
66 Disease outcomes are not always defined by *Avr/R* recognition events alone. Some
67 effectors suppress defence signalling or modulate host metabolic pathways to subvert
68 defence activation (Oliveira-Garcia et al., 2023; Ramírez-Zavaleta et al., 2022; Rhodes
69 et al., 2022). Defence suppressive effectors can be categorised into causing effector-
70 triggered susceptibility (ETS) or effector-triggered susceptibility II (ETS II), depending
71 on the molecular targets and their sequential effect during plant infection (Jones &

72 Dangl, 2006; Sohn et al., 2007; Win et al., 2012). ETS is defined as effector-
73 suppression of the defence response downstream of the recognition of conserved
74 pathogen molecules via pattern recognition receptors (Miya et al., 2007). ETS II is
75 defined as effector-suppression of defence signalling downstream of *Avr/R* recognition
76 events and can also be referred to as a 'recognize-then-suppress' model of plant-
77 pathogen interactions.
78 Despite significant progress in cloning wheat stripe rust *R* genes, the identification of
79 corresponding *Avr* genes in *Pst* has lagged far behind. To overcome these challenges,
80 we adapted and optimised a rapid protoplast-based screening system for functional
81 testing of *Pst* effector candidates (Wilson et al., 2024). We focused on hemizygous
82 effectors identified in the fully phased genome assembly of the Australian *Pst* isolate
83 Pst104E137A- (Tam et al., 2025). These effectors are of particular interest because
84 hemizygosity implies that only a single allele of an effector needs to undergo a
85 mutational event to avoid recognition in case of an avirulence effector. By screening
86 these previously identified hemizygous effectors, we isolated a single avirulence
87 effector candidate that is differentially recognised by a diverse set of wheat cultivars.
88 This study characterises this effector termed *AvrPstB48* and its four paralogs using a
89 protoplast screening system and diverse wheat cultivars. In addition to confirming their
90 recognition, we analysed *AvrPstB48* sequence diversity, expression patterns during
91 infection, recognition specificity and their potential impacts on disease outcome during
92 infection.
93

94 **MATERIAL AND METHODS**

95 **Candidate *Pst Avr* selection and gene synthesis**

96 Hemizygous effectors were previously identified by analysing a time course of long-
97 read transcriptomic datasets of Pst104E137A- as detailed in Tam et al. (2025). Briefly,
98 transcripts were sampled from six conditions, each with four replicates, including
99 ungerminated urediniospores and infected wheat leaves at 4, 6, 8, 10, and 12 days
100 post-infection (dpi). All samples were subjected to direct Oxford Nanopore
101 Technologies (ONT) cDNA sequencing. DESeq2 (Love et al., 2014) differential
102 expression analysis was conducted on transcript read abundance to identify
103 secretome genes upregulated ($\log_2$ fold change ≥ 2) early during infection (4 and 6
104 dpi) relative to dormancy. Inter-haplotype sequence analysis was then conducted to
105 shortlist the candidates based on hemizygosity. The selected candidates were
106 synthesised as gene blocks to facilitate precise assembly through Golden Gate cloning
107 (Engler et al., 2014). Here, we describe the functional characterisation of one of these
108 hemizygous effector candidates, ID Pst104E137_010232, referred to as *AvrPstB48*.
109

110 **Identification of *AvrPstB48* paralogs**

111 The tblastn v2.16.0+ was used to search for *AvrPstB48* paralogs using its protein
112 sequence against the *Pst*104E genome assembly (-evalue 1e-5) (Camacho et al.,
113 2009). We applied a low identity cut-off of 0.4, considering effector proteins are
114 typically sequence-divergent yet structurally conserved (Yu et al., 2023). The search
115 results were used to locate the annotated gene hits. Multiple protein sequence
116 alignments of *AvrPstB48* and the paralogs Pst104E137_025766 (*AvrPstB48_P1*),
117 Pst104E137_025767 (*AvrPstB48_P2*) and Pst104E137_010231 (*AvrPstB48_P3*),
118 were performed using MAFFT v7.490 (Katoh & Standley, 2013) and visually inspected
119 in Geneious to confirm overall similarities in physicochemical properties of individual
120 amino acids in the alignment.

121

122 **Effector prediction**

123 We used full-length protein sequences of *AvrPstB48, AvrPstB48_P1,*
124 *AvrPstB48_P2/P4*, and *AvrPstB48_P3* with SignalP6 to predict the presence and
125 location of signal peptides (Teufel et al., 2022). We used respective protein sequences
126 without signal peptide with EffectorP3 to predict the probability of the proteins to
127 encode for effectors, including preference for cytoplasmic and/or apoplastic effector
128 location (Sperschneider & Dodds, 2022).

129

130 ***In silico* structural modelling**

131 The predicted tertiary structures of *AvrPstB48* and its paralogs were generated using
132 the AlphaFold Server v3.0 (DeepMind, UK) (Abramson et al., 2024). Models were
133 generated based on the protein sequences with the signal peptides removed. The
134 predicted Template Modelling (pTM) score can be used to assess global model quality
135 and domain orientation, where scores ≥0.5 are generally considered acceptable for
136 reliable domain-level predictions (Jumper et al., 2021). The initial scores for all
137 structural models were <0.5 (Table S1). However, we observed from those models that
138 ~50 residues at the N-terminus of each protein were unstructured. We also noted that
139 the sequences of the proteins were rich in conserved cysteine residues. In other rust
140 effectors, these have been shown to co-ordinate Zn^{2+} (Zhang et al., 2018; Outram et
141 al., 2024). We therefore repeated the predictions with the N-terminal truncated and
142 Zn^{2+} included. We observed an overall improvement in the pTM scores for all models
143 >0.5 when the N-terminal region was removed, and the scores generally improved
144 further when Zn was added to the prediction. The interface prediction score for Zn
145 binding was, in most cases>0.7, indicating acceptable interaction/binding reliability

146 (Abramson et al., 2024) (Table S1). The resulting models were visualised and
147 analysed using PyMOL and ChimeraX v1.8 (UCSF) (Meng et al., 2023). Structural
148 comparison of *AvrPstB48* and its paralogs *(P1, P2/P4*, and *P3*) was performed via
149 superimposition in PyMOL, using *AvrPstB48* as the reference structure to identify
150 conformational differences that may underlie functional divergence (Table S1).
151

152 **Golden Gate assembly of expression constructs**

153 Synthetic double-stranded DNA fragments (gBlocks Gene Fragments; Integrated DNA
154 Technologies (IDT), Coralville, IA, USA) encoding the hemizygous effector candidate
155 *AvrPstB48*, its paralogs *AvrPstB48_P1*, *AvrPstB48_P2*, *AvrPstB48_P3*, and the
156 mutants *AvrPstB48*_D133G and *AvrPstB48_P3*_G133D were synthesised with
157 flanking *BsaI* recognition sites to generate an AATG overhang downstream of the long
158 intergenic region and a GCTT overhang upstream of the short intergenic region to
159 facilitate level 1 Golden Gate assemblies. The digested fragments were ligated into
160 the pWDV1 expression vector, which had also been digested with *BsaI*. The reaction
161 was cycled between 37°C for 3 minutes (to allow digestion) and 16°C for 4 minutes
162 (for ligation) for 25 cycles, followed by a final incubation at 50°C for 5 minutes and
163 80°C for 5 minutes to inactivate the *BsaI* enzyme. Following the Golden Gate reaction,
164 5 µL of the reaction mixture was transformed into competent *Escherichia coli* cells.
165 The cells were incubated on ice for 30 minutes, heat-shocked at 42°C for 30 seconds,
166 then returned to ice for 5 minutes. SOC medium (200 µL; containing 2% tryptone, 0.5%
167 yeast extract, 10 mM NaCl, 2.5 mM KCl, 10 mM $MgCl_2$, 10 mM $MgSO_4$, and 20 mM
168 glucose) was added, and the mixture was incubated at 37°C for 1 hour with shaking
169 at 250 rpm.

170 Transformed *E. coli* cells were plated on LB agar supplemented with 35 µg/mL
171 chloramphenicol and incubated overnight at 37°C. Individual colonies were screened
172 by colony PCR using gene-specific primers to confirm the presence of *Avr* candidate
173 inserts (Table S2). PCR-positive clones were cultured in LB broth for plasmid
174 extraction using a standard miniprep protocol (Qiagen). Extracted plasmids were
175 subjected to restriction enzyme digestion with insert-specific restriction sites to validate
176 correct plasmid architecture. Clones showing the expected digestion patterns were
177 then selected for full-length plasmid verification via ONT sequencing. Whole-plasmid
178 sequencing was performed using ONT MinION flow cells, and raw reads were
179 analysed in Geneious Prime v2025.1.3 using Minimap alignment against the plasmid
180 reference map to confirm correct insert orientation and base pair sequence integrity
181 (Li, 2018) (Table S3).
182

183 **Plant materials and growth conditions for protoplast isolation**

184 For each wheat cultivar (cv), Chinese 166, Avocet/*Yr1*, Heines VII, Nord Desprez,
185 *Triticum spelta*, Avocet/*Yr5*, Heines Peko, Heines Kolben, Avocet/*Yr6,* Reichersberg
186 42, Avocet/*Yr7*, Compare, Avocet/*Yr8,* Clement, Avocet/*Yr9*, *Yr15*, Avocet/*Yr15*,
187 Spalding prolific, Avocet/*YrSp*, Avocet S, Breakwell, Gabo, Coorong and Morocco, 15
188 seeds were sown in each pot (14 cm in diameter, 10 cm in depth, and approximately
189 1.5 L in volume). The plants were grown in controlled-environment growth cabinets at
190 18°C under a 16 h light/8 h dark photoperiod and a light intensity of 300 µmol/m²/s.
191 Relative humidity was maintained at 60% during the light period and 70% during the
192 dark period. Ten grams of soluble fertiliser (HORTICO) was dissolved in 4.5 L of water
193 and applied to each tray of plants. Plants were watered every two days. At 8 days after
194 sowing, leaves were harvested for protoplast isolation.

195

196 **Protoplast isolation**

197 Wheat protoplasts were isolated using the protocol described by Wilson et al. (2023,
198 2024), with minor modifications. Briefly, protoplasts were isolated by making shallow
199 incisions in the leaf epidermis of the first and second true leaf, followed by peeling the
200 epidermis to reveal the underlying mesophyll cells. The excised leaf segments were
201 incubated with the peeled surface in contact with a 0.6 M mannitol solution for 10
202 minutes. Subsequently, the segments were transferred to a Petri plate (4.5 cm)
203 containing an enzyme solution composed of MES buffer (pH 5.7, 20 mM), mannitol
204 (0.8 M), KCl (10 mM), cellulase (Yakult R-10) 1.5% w/v, macerozyme (Yakult R-10)
205 0.75% w/v, CaCl2 (10 mM), and BSA 0.1% w/v. The plate was wrapped in aluminium
206 foil to prevent light exposure and placed on an orbital shaker set to 60 rpm for 3 h at
207 room temperature. Following enzyme digestion, released protoplasts were filtered
208 through a 40 µm nylon cell strainer. Protoplasts were then collected from the enzyme
209 solution by gentle centrifugation at 100 g for 3 minutes using a 30 mL round-bottom
210 tube, resuspended and washed in W5 solution (MES buffer, pH 5.7, 2 mM; KCl, 5 mM;
211 $CaCl_2$, 125 mM; NaCl, 154 mM) and incubated at 4°C for 40 minutes to allow settling.,
212 A 10 µl aliquot of the concentrated protoplasts was taken for cell quantification and
213 quality assessment using a hemocytometer and light microscope. The protoplasts
214 were left at 4°C for 40 minutes to allow settling. The W5 solution was then removed,
215 and the protoplasts were resuspended to a final concentration of 300,000–350,000
216 cells/mL using MMG solution (MES buffer, pH 5.7, 4 mM; mannitol, 0.8 mM; $MgCl_2$, 15
217 mM). The protoplasts were used immediately for subsequent transfection.

218

219 **Protoplast transfection**

220 Plasmid DNA (1 µg/µL) was prepared using standard mini and maxi-prep protocols
221 (SV Wizard kits, Promega, Madison, WI, USA). Protoplast isolation and PEG-mediated
222 transfection followed the method described by Wilson et al. (2024), adapted to a 96-
223 well plate format to increase scalability and throughput (Khan et al., 2022; Lloyd et al.,
224 2022) with additional optimizations (Pereira et al., 2025).
225 All expression constructs were based on the self-replicating pWDV1 vector backbone
226 and were driven by the maize ubiquitin (UBI) promoter (Table S3). This included (i)
227 individual *Avr* effector candidates, (ii) wheat resistance (*R*) genes of positive control
228 Sr50, and (iii) luciferase reporter constructs. Reporter activity was quantified using a
229 dual-luciferase system adapted from Wilson et al. (2024), in which a defence-inducible
230 reporter plasmid (UBI-pDefense) and a constitutive normalisation plasmid (UBI-pRedf)
231 were co-transfected. These reporters use the same substrate but encode luciferases
232 with distinct emission spectra, which were read using dedicated Lumi Green band-
233 pass (~505 – 560 nm) and Red NB long-pass (cut-on ~600 nm) filters on a
234 luminescence plate reader (Tecan, Mannedorf, Switzerland; Infinite 200Pro) to allow
235 ratiometric normalisation of defence induction.
236 For each transfection, three classes of reactions were prepared in parallel: (i) *Avr*
237 candidates under test, (ii) a positive control (*AvrSr50* + Sr50), and (iii) a negative
238 control (*AvrSr50* alone, no matching *R* gene). In positive-control wells, 0.5 µg of the
239 *AvrSr50* effector plasmid, 2 µg of the Sr50 resistance gene plasmid, and 5 µg of each
240 reporter plasmid (UBI-pDefense and UBI-pRedf) were co-transfected per well.
241 Negative-control wells received 0.5 µg of the *AvrSr50* plasmid plus 5 µg of each
242 reporter plasmid but no *Sr50* plasmid, to confirm that defence reporter activation
243 required a cognate *R* gene. *Avr*-only reactions for candidate effectors were assembled
244 analogously, using 1 µg of the *Avr* candidate plasmid and 5 µg of each reporter

245 plasmid, without an *R* gene. Plasmid DNA mixes were dispensed into sterile 96-well
246 V-bottom plates (Costar). Freshly isolated wheat protoplasts (50 µL per well) were
247 added, followed by 50 µL of PEG solution (40% w/v PEG 4000, 0.2 M mannitol, 100
248 mM $CaCl_2$). The suspension was gently mixed by pipetting up and down five times,
249 then incubated for 10 min at room temperature to allow DNA uptake. Transfection was
250 stopped by adding 200 µL of W5 solution (154 mM NaCl, 125 mM $CaCl_2$, 5 mM KCl,
251 2 mM MES, pH 5.7). The plates were then incubated under low-light conditions at room
252 temperature for 16 h to permit expression prior to luminescence quantification.
253

254 **Monitoring luciferase expression**

255 After the 16h incubation, protoplasts were prepared for luminescence measurement.
256 The W5 supernatant was removed gently using a multichannel pipette without
257 disturbing the settled protoplast pellet. Fifty µL of 1× cell lysis buffer (#E3971;
258 Promega) was added, and the samples were gently mixed by pipetting 5 times, then
259 incubated for 15 minutes to ensure complete lysis. Fifty µL of lysate was collected and
260 transferred to an opaque, flat-bottom, white, solid polystyrene 96-well plate (Corning
261 96-well NBS Microplate, #CLS3600). The total luminescence was measured using a
262 plate reader (Tecan, Mannedorf, Switzerland; Infinite 200Pro, 1000 ms integration,
263 0 ms settle) without adding substrate to measure background signal. Immediately after
264 this baseline read, 50 µL of Steady-Glo luciferase substrate (Promega, #E2520) was
265 added to each well, and the luminescence was measured again. The plate reader was
266 programmed first to measure total luminescence without filters, using an integration
267 time of 1000 ms and a settle time of 0 ms. Subsequently, luminescence was recorded
268 sequentially through the installed Lumi Green band-pass (~505–560 nm) and Red NB
269 long-pass (cut-on ~600 nm) filters under the same acquisition settings. These filtered

270 measurements allowed separation of the defence-inducible reporter (UBI-pDefense)
271 and the constitutive normalisation reporter (UBI-pRedf), which use the same substrate
272 but emit at different wavelengths.
273

274 **Protoplast RT-PCR**

275 Wheat protoplasts were prepared as described above and dispensed at 900 µL per
276 replicate (3.5×10^5 cells mL^{-1} in MMG buffer) for transfection. For each transfection,
277 9 µg of the candidate expression plasmid was co-transfected with 5 µg of each
278 reporter. Transfections were performed in four independent biological replicates. After
279 16 h at room temperature under low light, 50 µL of each suspension was removed for
280 luciferase quantification, and the remaining protoplasts were pelleted by centrifugation
281 at 300 x g for 3 min. The supernatant was removed, snap-frozen in liquid nitrogen, and
282 stored at −80 °C for RNA extraction.
283 Total RNA was isolated with the Direct-zol RNA MiniPrep Plus kit (Zymo Research)
284 following the manufacturer's instructions, including on-column DNase I treatment.
285 RNA integrity was verified by agarose gel electrophoresis, and concentration and
286 purity were measured with a Qubit fluorometer and a NanoDrop spectrophotometer.
287 For cDNA synthesis, 1 µg of total RNA was reverse-transcribed using the High-
288 Capacity cDNA Reverse Transcription Kit (Thermo Fisher Scientific) according to the
289 manufacturer's protocol.
290 Gene-specific primers targeting *AvrPstB48* and the paralog *AvrPstB48_P3* were
291 designed in Geneious. Wheat 18S rRNA (Ta-18S) primers served as an endogenous
292 reference control (Table S2).
293 Conventional endpoint RT-PCR was performed with GoTaq DNA polymerase
294 (Promega) in 10 µL reactions with 3 µL cDNA template. Thermal cycling used a

295 standard program (1 cycle of 95 °C for 1 min and 30 s; 30 cycles of 95 °C for 30 s,
296 primer-specific annealing temperature of 50 °C for 30 s, and 72 °C for 2 min; final
297 extension 72 °C for 5 min). Empty-vector (EV) transfections were included as negative
298 biological controls; no-template controls (NTC) were run for each primer pair.
299 Amplicons (5 µL per reaction) were resolved on 1% agarose in 1× TAE, stained, and
300 imaged alongside a 1 kb Plus DNA Ladder (NEB #N3200).

301

302 **Inoculation of wheat plants with *Pst***

303 Fresh spores of *Pst* isolate Pst104E137A- (Schwessinger et al., 2018) were collected
304 from infected leaf tissue. Spores were suspended in 3M Novec solution and measured
305 using a CellDrop Automated Cell Counter (DeNovix Inc.) to a concentration of
306 approximately 5×10^5 spores/mL. Using a paintbrush, spores were inoculated on the
307 upper surface of the first-emerged leaf of wheat cv Avocet *S* and Morocco 14 days
308 after sowing at the same conditions described above. Infected plants were lightly
309 sprayed with clean deionised water before being placed in an opaque, 25-L plastic
310 container (33 cm x 22.5 cm x 47 cm) with a lid. Containers with infected plants were
311 wrapped with black plastic bags and incubated at 10°C in the dark to initiate *Pst*
312 germination. After 48 hours, the infected plants were removed from the container and
313 transferred back to the growth cabinet. Each infected leaf was assessed according to
314 Dracatos et al. (2016) over 10 or more days post-infection (dpi).

315

316 **Hyphae staining of infected wheat leaves**

317 Staining was performed as described by Redkar *et al.* (2018). Freshly harvested leaf
318 tissues were placed in 2 mL tubes containing 100% ethanol for three days or until the
319 majority of the chlorophyll had been removed. When the tissues were nearly devoid of

320 colour, ethanol was replaced with 10% aqueous potassium hydroxide and incubated
321 on a dry heating block at 85°C for two hours. Cleared tissues were carefully washed
322 10 times in 1x phosphate-buffered saline (PBS Thermo Fisher Scientific, 28237), pH
323 7.4. Propidium iodide (PI; Sigma-Aldrich, P4170) was mixed with wheat germ
324 agglutinin conjugated with AlexaFluor488 (WGA-AF488; Thermo Fisher Scientific,
325 W11261) to create a PI-WGA AF488 staining solution (20 µg/mL PI, 10 µg/mL WGA-
326 AF488, and 0.1% Tween 20 in 1× PBS, pH 7.4). After discarding the last PBS wash,
327 PI-WGA-AF488 staining solution was added to the 2 mL tubes to fully submerge the
328 tissues. Vacuum infiltration was applied at 7 millibars, repeated 5 times for 2 minutes
329 each, with 2-minute vacuum release in between. Stained tissues were washed twice
330 in 1x PBS to remove excess staining solution, transferred to fresh 1x PBS and stored
331 at 4°C in the dark.

332

333 **Callose staining of infected wheat leaves**

334 Freshly harvested leaf tissues were placed in 2 mL tubes containing 1x PBS, pH 7.4
335 and vacuum infiltrated at 7 millibars until they sank to the bottom of the tube. Prior to
336 staining, leaf tissues were hand-sectioned paradermally using a razor blade. Eight
337 pieces of sectioned leaf tissue were placed in each well of the 96-well plate and
338 washed with 200 µL 1x PBS. Tissues were stained with 0.1% aniline blue (AB; Sigma-
339 Aldrich, 415049) in 1x PBS for 60 mins with vacuum infiltration and washed twice in
340 1x PBS. WGA-AF488 staining solution (10 µg/L WGA-AF488 and 0.1% Tween 20 in
341 1× PBS, pH 7.4) was added to the samples and vacuum infiltrated at 7 millibars for 5
342 times, 2 minutes each, with 2-minute vacuum release in between. Samples were
343 washed twice in 1x PBS, transferred to fresh 1x PBS and stored at 4°C in the dark.

344

345 **Confocal fluorescence microscopy**

346 Stained leaf tissues were mounted onto a glass slide with 1x PBS and imaged under
347 a TCS SP8 confocal microscope (Leica Microsystems) using 20x (PI-WGA-AF488)
348 and 63x (AB-WGA-AF488) water-immersion objectives. WGA-AF488-stained fungal
349 structures were visualised at 500-540 nm following excitation with an Argon laser at
350 488 nm. PI-stained cell wall was visualised at 580-630 nm following excitation with a
351 DPSS laser at 561 nm. AB-stained callose was visualised at 430-500 nm following UV
352 excitation at 405 nm. To obtain a composite image with greater depth of field, Z-
353 stacking was performed with each optical section captured at a 0.1 µm interval. Images
354 were processed (e.g., maximum projection, brightness and contrast) using Leica
355 Application Suite X software (LASX, Leica Microsystems).

356

357 **Data collection and statistical analysis**

358 Differences in normalised luminescence values were assessed using one-way
359 analysis of variance (ANOVA) followed by Tukey's Honestly Significant Difference
360 (HSD) post hoc test (Wilson et al., 2024). The infectious hyphae cover area per leaf
361 surface area was quantified using images obtained from PI-WGA-AF488-stained leaf
362 tissues. Meanwhile, the callose signal area was quantified using images obtained from
363 AB-WGA-AF488-stained leaf tissues. These quantifications were performed using
364 ImageJ software (National Institutes of Health) on a Wacom Cintiq graphics tablet
365 (Wacom Technology). Statistical analysis of data obtained from confocal images was
366 performed using Welch's t-test.

367

368 **RESULTS**

369 **A hemizygous stripe rust candidate effector triggers defence signalling in wheat**
370 **protoplasts**

371 The hemizygous effector candidates were identified previously from the nuclear
372 haplotype-phased genome of the *Pst* reference isolate Pst104E137A- (Tam et al.,
373 2025). Here we describe the functional characterisation of one of these hemizygous
374 effector candidates referred to here as *AvrPstB48*. The name *AvrPstB48* reflects its
375 predicted avirulence function “Avr” in *Pst*, with “B” representing its broad recognition
376 pattern across diverse wheat cultivars, and “48” corresponding to its internal candidate
377 ID in the screening pipeline. Additional hemizygous effector candidates, including
378 *Pst104E137_008104* (#47) and *Pst104E137_024713* (#49), were selected using the
379 same criteria and served as comparisons for validation assays (Tam et al., 2025).
380 Because *AvrPstB48* expression pattern aligned with a function during plant infection
381 (Tam et al., 2025), we cross-validated its role as effector using the machine learning
382 tool EffectorP3 (Sperschneider & Dodds, 2022). *AvrPstB48* was predicted as an
383 effector with a most likely intracellular localisation. We therefore decided to perform
384 transient expression of *AvrPstB48* in wheat protoplasts with its signal peptide removed
385 to allow for intracellular localisation. Using a dual luciferase-based defence reporter
386 assay with the D14 defence promoter (Wilson et al., 2024), we observed a robust and
387 specific increase in ratiometric luminescence following co-expression of *AvrPstB48*
388 and the defence reporter, indicating a recognition-dependent defence response in
389 Avocet *Yr5* and Avocet *S* (Figure 1). The increase in ratiometric luminescence
390 observed when expressing *AvrPstB48* was similar to the *AvrSr50/Sr50* gene pair,
391 which served as a positive control to validate the assay performance (Wilson et al.,
392 2024). By contrast, two other hemizygous effector candidates, #47 and #49, did not

393 induce measurable reporter activity being similar to the negative control, *AvrSr50*
394 (Figure 1). Together, these results are consistent with *AvrPstB48* encoding a
395 recognised effector activating host defence responses in specific wheat cultivars
396 (Table S5).
397 Given the strong defence promoter activation observed for *AvrPstB48*, further analysis
398 was conducted to identify and characterise its paralogs. Sequence homology analysis
399 was performed by tblastn and revealed two divergent paralogs located in close
400 proximity on each haplotype of chromosome 10, *AvrPstB48*_P1, *AvrPstB48*_P2,
401 *AvrPstB48_P3* and *AvrPstB48*_P4. Among these allelic pairs, *AvrPstB48*_P2 and
402 *AvrPstB48*_P4 share 100% nucleotide identity, whereas *AvrPstB48*_P1 and
403 *AvrPstB48_P3* exhibit 98.2% nucleotide identity. Relative to AvrPstB48, the *P2/P4* pair
404 is more closely related (90.8%), whereas the *P1/P3* pair is more divergent (57.6%
405 identity to *AvrPstB48_P1*) (Figure 2a). Consistent with this, protein sequence
406 alignments show that AvrPstB48_P2/P4 are highly similar to AvrPstB48, whereas
407 AvrPstB48_P1 and AvrPstB48_P3 carry multiple non-synonymous substitutions and
408 are more divergent at the amino-acid level (Figure 2b). AlphaFold3 modelling
409 supported a shared fold among AvrPstB48, P1, P2/4, and P3. Backbone superposition
410 yielded pairwise RMSDs of ~0.5–1.5 Å, with divergence concentrated in the C-terminal
411 helical region and adjacent loops (Fig. 2c). Global pTM values (≈0.50–0.57) indicate
412 these are hypothesis-generating rather than definitive models; nevertheless, they are
413 consistent with a conserved core and local surface variation between the paralogs.
414 The locations of these variations correspond to clusters of substitutions in the multiple
415 sequence alignment (Fig. 2b) and may modulate protein stability or interactions with
416 host targets. Temporal expression profiling across infection stages revealed distinct
417 expression patterns among the paralogs (Figure 2d). *AvrPstB48* exhibited peak

418 expression at 8 days post-inoculation (dpi), reaching its highest levels relative to the
419 other paralogs. All paralogs also peaked at 8 dpi, although expression intensity varied,
420 with *P1*, *P2/P4*, and *P3* remaining moderately expressed throughout the infection time
421 course. None of the paralogs were expressed in ungerminated spores, supporting their
422 likely function in host-pathogen interactions.
423

424 ***AvrPstB48* recognition is conserved across multiple wheat cultivars**

425 To further assess defence promoter activation triggered by *AvrPstB48*, we tested their
426 activities in additional wheat cultivars including Avocet S, Morocco, *Triticum spelta Yr5*,
427 Chinese 166 and Gabo, using three previously validated defence reporter promoters
428 (D2, D14, and D15) (Wilson et al., 2024). Significant activation of each promoter was
429 observed in response to *AvrPstB48* expression in Avocet *S* (Figure 3a), *T. spelta Yr5*
430 and Gabo (Figures S1a, S1b), indicating effector recognition. In contrast, no increase
431 in ratiometric luminescence signal was detected in Morocco (Figure 3b) or Chinese
432 166 (Figure S1c), suggesting a lack of *AvrPstB48* recognition in these cultivars.
433 Additional screening of 16 wheat cultivars confirmed consistent activation in all near-
434 isogenic Avocet lines, while eight cultivars showed no measurable response (Table
435 S5). Importantly, the positive control (*AvrSr50/Sr50*) consistently induced strong
436 luminescence across all tested backgrounds, validating assay performance.
437

438 ***AvrPstB48* paralogs *AvrPstB48_P1* and *AvrPstB48_P2/P4,* but not**
439 ***AvrPstB48_P3,* are recognized in multiple wheat cultivars**

440 To assess the functional redundancy of *AvrPstB48*, we tested recognition of its
441 paralogs in the same set of wheat cultivars, Avocet S, Morocco, *T. spelta Yr5*, Gabo,
442 and Chinese 166, using activation of the D14 promoter as a readout. Defence

443 activation was detected for *AvrPstB48*_P1 and *AvrPstB48*_P2/P4 in Avocet *S* (Figure
444 4a), *T. spelta Yr5,* and Gabo (Figures S2), suggesting a similar recognition spectrum
445 to *AvrPstB48*. *AvrPstB48_P3* failed to activate the D14 defence promoter in any of the
446 tested cultivars. No induction was observed for any of the paralogs tested in Morocco
447 (Figure 4b) and Chinese 166 (Figure S2).
448 Given that *AvrPstB48_P3* shares overall structural and sequence similarity with
449 *AvrPstB48* (Figure 2), we investigated whether it could interfere with *AvrPstB48*-
450 triggered defence signalling. In co-expression assays in Avocet *S* protoplasts,
451 *AvrPstB48* was delivered either alone or together with *AvrPstB48*_P3 at a 1:1 plasmid
452 ratio. Co-expression did not reduce relative ratiometric luminescence signal induction
453 when compared to *AvrPstB48* alone, indicating that *AvrPstB48_P3* does not act as a
454 competitive suppressive paralog when co-expressed in wheat protoplasts (Figure 4c).
455 To verify effector transcript accumulation for both *AvrPstB48* and *AvrPstB48_P3*, we
456 performed endpoint RT-PCR on cDNA from protoplasts transfected with the
457 corresponding expression constructs. Gene-specific primer pairs yielded the expected
458 amplicons for *AvrPstB48* and *AvrPstB48_P3* only in the matched transfection. No
459 bands were detected in empty vector (EV) controls amplified with either primer set.
460 The wheat 18S rRNA control amplified in all samples, supporting cDNA quality (Figure
461 S3).
462

463 **Aspartic acid at position 134 is necessary but not sufficient for defence**
464 **activation**

465 To investigate why *AvrPstB48_P3* does not trigger defence promoter activation in
466 Avocet S, we explored potential structural and biochemical differences among
467 *AvrPstB48* and its paralogs. Structural predictions using AlphaFold3 revealed that all

468 paralogs adopt a broadly conserved fold (Figure 2d). Closer inspection revealed
469 several amino acid substitutions specific to *AvrPstB48_P3*, particularly in surface-
470 exposed loops that may be involved in effector recognition and receptor interactions.
471 One notable difference occurs at position 134, where *AvrPstB48, AvrPstB48_P1*, and
472 *AvrPstB48_P2* encode an aspartic acid (D), while *AvrPstB48_P3* encodes a glycine
473 (G) (Figure 5a). This substitution replaces a negatively charged residue (D) with a
474 small, nonpolar amino acid (G) at a position that is predicted to be surface-exposed
475 on a protruding loop. This makes the D134G substitution a prime candidate for
476 functional testing.
477 To further investigate the functional significance of the amino acid variation at position
478 134, synthetic gene fragments were designed to encode *AvrPstB48* carrying an
479 aspartic acid to glycine substitution (D134G), and *AvrPstB48_P3* carrying the reverse
480 substitution (G134D). These constructs were tested for their ability to induce defence
481 promoter activation in Avocet *S* using the D14 promoter-luciferase reporter system in
482 wheat protoplasts. AvrPstB48_D134G failed to activate the defence reporter when
483 compared to the increase of ratiometric luminescence when expressing wild-type
484 *AvrPstB48* (Figure 5b). This indicates that the D134G substitution is sufficient to
485 disrupt recognition. The reciprocal mutant AvrPstB48_P3_G134D also failed to induce
486 defence promoter activity, suggesting that the aspartic acid at position 134 is not the
487 only residue contributing to the avoidance of recognition in *AvrPstB48_P3*.
488

489 ***AvrPstB48*-triggered reporter activation in protoplasts does not correlate fully**
490 **with *Pst* resistance *in planta***

491 We assessed infection outcomes using the Australian pathotype Pst104E137A-
492 (Schwessinger et al., 2018) to evaluate whether the *AvrPstB48*-triggered reporter

493 activation observed in wheat protoplasts corresponded to resistance *in planta*. Wheat
494 lines previously tested in the protoplast assay were inoculated and disease severity
495 scored at 10 days post-inoculation (dpi) using a 0–9 infection type (IT) scale
496 (Hovmøller et al., 2017). Reporter activation in protoplasts did not correlate with
497 disease outcomes in all cultivars tested. While *T. spelta Yr5* and Chinese 166 exhibited
498 full resistance (IT = 0), Gabo, Morocco, and Avocet *S* were highly susceptible (IT = 9),
499 despite *AvrPstB48* triggering defence promoter activation in Gabo and Avocet *S*
500 (Figure S4).

501

502 **_AvrPstB48_ recognition correlates with delayed infection progression in the**
503 **susceptible wheat cultivar Avocet S**

504 To explore whether *AvrPstB48* recognition might influence infection dynamics even in
505 a susceptible genotype, we compared Avocet *S* and Morocco. Both of these are
506 susceptible to the *Pst* isolate Pst104E137A-, but Avocet *S* responds to *AvrPstB48*
507 expression in the protoplast assay, whereas Morocco does not. At 8 dpi, neither line
508 exhibited macroscopic ureodiniospore formation. By 10 dpi, both displayed visible rust
509 symptoms, however, Morocco developed more extensive ureodiniospore coverage,
510 indicating a higher sporulation capacity and greater disease severity (Figure 6A).
511 Confocal microscopy supported these observations, revealing more abundant and
512 earlier hyphal growth in Morocco compared to Avocet *S* at 8 dpi (Figure 6B). Although
513 both lines were heavily colonised by 10 dpi, Avocet *S* retained localised areas with
514 reduced fungal presence, consistent with greater disease severity. Quantification of
515 infectious hyphal cover over time showed broadly similar colonisation dynamics

516 between the two genotypes, with Morocco tending to exhibit slightly higher mean
517 hyphal coverage at later time points (Figure 6D).
518 To assess host immune responses underlying these differences, we examined callose
519 deposition, a hallmark of plant defence. At 8 dpi, Avocet *S* exhibited greater callose
520 accumulation than Morocco, particularly around infection sites (Figure 6C), and this
521 was supported by quantitative analysis (Figure 6E).

522

523 **Discussion**

524 Recent advances in high-quality genome assemblies of *Pst* (Wang et al., 2024; Tam
525 et al., 2025), coupled with advances in effector identification and functional genomics,
526 have significantly enhanced our capacity to investigate host–pathogen interactions of
527 *Pst* and other rust wheat rust fungi (Arndell et al., 2024; Chen et al., 2017; Chen et al.,
528 2024; Cui et al., 2024; Outram et al., 2024; Salcedo et al., 2017; Shen et al., 2024;
529 Upadhyaya et al., 2021; Wilson et al., 2024). Additionally, we have gained deeper
530 insights into wheat defence responses by integrating comprehensive effector libraries
531 with protoplast transient expression methods (Arndell et al., 2024; Wilson et al., 2024).
532 Within this framework, we identified *AvrPstB48* as a hemizygous avirulence candidate
533 effector that triggers defence signalling in a wheat cultivar-specific manner. Using
534 wheat protoplasts, we deliberately focused on intracellular expression of *AvrPstB48,*
535 removing the signal peptide encoding sequence from the expression clone based on
536 localisation prediction made with EffectorP3. In cultivars such as Avocet *S, T. spelta*
537 *Yr5* and Gabo, intracellular expression of *AvrPstB48* elicited strong activation of
538 defence reporters, comparable in magnitude to the canonical *Avr/R* control
539 *AvrSr50/Sr50*, whereas Morocco and Chinese 166 showed no detectable response to

540 *AvrPstB48*. This clear cultivar-specific response and its intracellular recognition align
541 with intracellular *R* gene-mediated recognition in wheat protoplasts and mirror prior
542 observations *for AvrSr35, AvrSr27, AvrSr13, AvrSr22* and *AvrPm2a*, all of which
543 activate the same defence reporters in protoplasts when expressed in the presence of
544 their cognate *R* genes (Wilson et al., 2024). While we have not identified a cognate *R*
545 gene for *AvrPstB48*, we hypothesise that it is recognised by a broadly conserved *R*
546 gene that is common to the wheat cultivars that respond to *AvrPstB48*. Importantly,
547 the cultivar-specific recognition of *AvrPstB48* did not correlate with full disease
548 resistance when using the *AvrPstB48*-encoding isolate Pst104E137A– for infection
549 assays. Several cultivars that responded to *AvrPstB48* with defence signalling in
550 protoplasts, such as Avocet S and Gabo, were fully susceptible in whole plant infection
551 assays at 14 dpi.
552 We chose Avocet *S* and Morocco for more detailed phenotypic comparisons of two
553 fully susceptible wheat cultivars that varied in their response to *AvrPstB48*. We
554 selected them because they are both widely used as 'universal' susceptible *Pst*
555 cultivars*,* with the key difference that there are recent reports of *Pst* isolates that are
556 avirulent on Avocet *S* (Nazari & El Amil, 2014) but not on Morocco. Based on this
557 observation, there was justification to postulate that Avocet *S* carries a *R* gene
558 designated *YrAvS* that is observable only during whole plant infection assays and with
559 certain *Pst* isolates. We did observe a lower sporulation and hyphal coverage in Avocet
560 *S* when compared to Morocco in our detailed macroscopic and microscopic time
561 course infection comparison using Pst104E137A-. This infection delay in Avocet *S* is
562 consistent with its ability to recognise *AvrPstB48,* upon which we propose the
563 presence of the uncharacterised *YrAvS*. We do not know if *AvrPstB48* recognition
564 contributes to infection delay and if it is recognised by *YrAvS*. An infection delay could

565 also be caused by the recognition of another effector by *YrAvS* or any other unrelated
566 genetic differences between Avocet *S* and Morocco. However, it is tempting to
567 speculate that the recognition of *AvrPstB48* contributes to the infection delay, because
568 recent segregation analysis of a *PstS8* selfing population suggests the presence of an
569 effector that can suppress the recognition of *PstS8* on Avocet *S*, rendering *PstS8*
570 virulent despite the presence of an avirulence effector (Livbjerg et al., 2025). Similar
571 observations of "inhibitor" loci that suppress *Avr* recognition have been made for the
572 flax rust fungus *Melampsora lini* (Lawrence et al., 1981) and the barley powdery
573 mildew fungus *Blumeria graminis* f. sp. *hordei* (Caffier et al., 1996). These are
574 consistent with a recent observation in which some *Blumeria graminis* f. sp. *tritici*
575 isolates employ the effector SvrPm4 to suppress the recognition of AvrPm4 by Pm4
576 (Bernasconi et al., 2025). We therefore hypothesise that the *AvrPstB48*-Avocet *S*
577 phenotype is explained by a 'recognise–then–suppress' scenario, fitting within the
578 concept of ETSII. In ETSII, effectors that are poised to trigger *R* gene dependent
579 disease resistance are attenuated by other effectors that suppress defence signalling,
580 allowing disease progression despite recognition (Sohn et al., 2007; Wu & Derevnina,
581 2023). Therefore, the infection outcomes of the *Pst*-wheat pathosystem are likely more
582 complex than Flor's gene-for-gene hypothesis suggests (Flor, 1971), reflecting the
583 complex coevolution between the obligate biotroph pathogen and its host.
584 Paralog analysis revealed that *AvrPstB48* belongs to a small effector family with four
585 out of five members triggering host defence. Two paralogs (*P1* and *P2/P4*) trigger
586 defence activation in *AvrPstB48* responsive cultivars, whereas *P3* consistently did not.
587 *AvrPstB48_P3* provides an example of how local sequence changes within a shared
588 scaffold mediate escape from recognition. Structural modelling and mutational
589 analyses identified the single amino acid at position 134 as a key determinant of

590 recognition. In AvrPstB48, P1 and P2/P4, this position encodes an aspartic acid
591 (D134), whereas P3 encodes a glycine (G134). AlphaFold-based models predict that
592 residue 134 lies within a solvent-exposed loop projecting from a compact, cysteine-
593 rich core. Replacing D134 with G134 in AvrPstB48 abolished defence activation,
594 whereas the reciprocal G134 to D134 change in P3 failed to restore recognition. This
595 asymmetry indicates that D134 is necessary but not sufficient for recognition. The
596 predicted *AvrPstB48* fold, a compact, cysteine-rich core likely stabilised by disulphide
597 bonds and Zn^{2+} coordination decorated with variable surface loops, is consistent with
598 emerging paradigms for rust effectors such as *AvrSr27*, in which conserved cysteines
599 and metal-binding centres maintain the core, while modular loops control host
600 specificity and escape (Outram et al., 2024).
601

602 **Acknowledgments**

603 We acknowledge the contribution of the Plant Pathogen 'Omics Initiative consortium
604 in the generation of data used in this publication. The Initiative is supported by funding
605 from Bioplatforms Australia, enabled by the Commonwealth Government National
606 Collaborative Research Infrastructure Strategy (NCRIS).

607 **Author contributions:** B.S., B.D., R.T., and J.P.R. conceptualized the project. B.S.,
608 R.T. and J.P.R. acquired funding. B.S. supervised the work. E.C.P., B.D., R.T., H.L.,
609 D.I.B., M.M., M.R., S.W., S.P., and F.D. acquired experimental data and conducted
610 data analysis. E.C.P. and B.S. drafted the manuscript, and all authors contributed to
611 writing, reviewing, and editing.

612 **Data availability:** All supporting data is available on Zenodo (doi:
613 10.5281/zenodo.15845412, link: 10.5281/zenodo.15845412).

614 **Funding:** This work was supported by a Discovery Project grant from the Australian
615 Research Council (DP230100941) to B. S. and J. P. R. This work was supported by
616 computational resources provided by the Australian Government through the National
617 Computational Infrastructure (NCI) under the ANU Merit Allocation Scheme. R.T. was
618 supported by a Grains Research and Development Corporation Graduate Research
619 Scholarship.

620 **References**

621 Abramson, J., Adler, J., Dunger, J., Evans, R., Green, T., Pritzel, A., Ronneberger, O.,
622 Willmore, L., Ballard, A.J., Bambrick, J., Bodenstein, S.W., Evans, D.A., Hung,
623 C.C., O'Neill, M., Reiman, D., Tunyasuvunakool, K., Wu, Z., Žemgulytė, A.,
624 Arvaniti, E., Beattie, C., Bertolli, O., Bridgland, A., Cherepanov, A., Congreve, M.,
625 Cowen-Rivers, A.I., Cowie, A., Figurnov, M., Fuchs, F.B., Gladman, H., Jain, R.,
626 Khan, Y.A., Low, C.M.R., Perlin, K., Potapenko, A., Savy, P., Singh, S., Stecula, A.,
627 Thillaisundaram, A., Tong, C., Yakneen, S., Zhong, E.D., Zielinski, M., Žídek, A.,
628 Bapst, V., Kohli, P., Jaderberg, M., Hassabis, D., and Jumper, J.M. 2024.
629 Addendum: Accurate structure prediction of biomolecular interactions with
630 AlphaFold 3. Nature. 636: E4.

631 Amezrou, R., Audeon, C., Compain, J., Gelisse, S., Ducasse, A., Saintenac, C.,
632 Lapalu, N., Louet, C., Orford, S., Croll, D., Amselem, J, Fillinger, S, and Marcel,
633 T.C. 2023. A secreted protease-like protein in *Zymoseptoria tritici* is responsible
634 for avirulence on Stb9 resistance gene in wheat. PLoS Pathog. 19: e1011376.

635 Arndell, T., Chen, J., Sperschneider, J., Upadhyaya, N.M., Blundell, C., Niesner, N.,
636 Outram, M.A., Wang, A., Swain, S., Luo, M., Ayliffe, M.A., Figueroa, M.,
637 Vanhercke, T., and Dodds, P.N. 2024. Pooled effector library screening in
638 protoplasts rapidly identifies novel *Avr* genes. Nat. Plants 10: 572–580.

639 Bernasconi, Z., Herger, A.G., Caro, M.D.P., Kunz, L., Müller, M.C., Stirnemann, U.,
640 Outram, M.A., Widrig, V., Neidhart, M., Isaksson, J., Schudel, S., Rösli, S., Wicker,
641 T., Bender, K.W., Zipfel, C., Dodds, P.N., Figueroa, M., Sánchez-Martín, J., and
642 Keller, B. 2025. Virulence on Pm4 kinase-based resistance is determined by two
643 divergent wheat powdery mildew effectors. bioRxiv 2025.07.04.663163.
644 doi:10.1101/2025.07.04.663163

645 Bourras, S., Kunz, L., Xue, M., Praz, C.R., Muller, M.C., Kälin, C., Schläfli, M.,
646 Ackermann, P., Flückiger, S., Parlange, F., Menardo, F., Schaefer, L.K., Ben-
647 David, R., Roffler, S., Oberhaensli, S., Widrig, V., Lindner, S., Isaksson, J., Wicker,
648 T., Yu, D., and Keller, B. 2019. The *Avr*Pm3-Pm3 effector-NLR interactions control
649 both race-specific resistance and host specificity of cereal mildews on wheat. Nat.
650 Commun. 10: 2292.

651 Caffier, V., de Vallavieille-Pope, C., and Brown, J.K.M. 1996. Segregation of
652 avirulences and genetic basis of infection types in *Erysiphe graminis f. sp. hordei*.
653 Phytopathol. 86:1112–1121.

654 Camacho, C., Coulouris, G., Avagyan, V., Ma, N., Papadopoulos, J., Bealer, K., and
655 Madden, T.L. 2009. BLAST+: architecture and applications. BMC Bioinform. 10:
656 421.

657 Chen, J., Upadhyaya, N.M., Ortiz, D., Sperschneider, J., Li, F., Bouton, C., Breen, S.,
658 Dong, C., Xu, B., Zhang, X., Mago, R., Newell K, Xia, X., Bernoux, M., Taylor, J.M.,
659 Steffenson, B., Jin, Y., Zhang, P., Kanyuka, K., Figueroa, M., Ellis, J.G., Park, R.F.,
660 and Dodds, P.N. 2017. Loss of *Avr*Sr50 by somatic exchange in stem rust leads
661 to virulence for Sr50 resistance in wheat. Science 358: 1607–1610.

662 Chen, R., Chen, J., Outram, M.A., Powell, O.R., Arndell, T., Gajendiran, K., Wang, Y.L.,
663 Ayliffe, M.A., Blundell, C., Figueroa, M., Sperschneider, J., Vanhercke, T., Tang,
664 D., Xu, Y., Zhong, G., Gardener, C., Yu, G., Gourdoupis, S., Jaremko, Ł., Matny,
665 O., Steffenson, B.J., Boshoff, W.H.P., Meyer, W.B., Arold, S.T., Dodds, P.N., and
666 Wulff, B.B.H. 2024. A wheat tandem kinase sensor activates an NLR helper to
667 trigger immunity. Science 387: 1402-1408.

668 Cui, Z., Shen, S., Meng, L., Sun, X., Jin, Y., Liu, Y., Liu, D., Ma, L., and Wang, H. 2024.
669 Evasion of wheat resistance gene *Lr15* recognition by the leaf rust fungus is
670 attributed to the coincidence of natural mutations and deletion in *AvrLr15* gene.
671 Mol. Plant Pathol. 25: e13490.

672 Derbyshire, M.C., and Raffaele, S. 2023. Surface frustration re-patterning underlies
673 the structural landscape and evolvability of fungal orphan candidate effectors. Nat
674 Commun. 14:5244.

675 Dodds, P.N., and Rathjen, J.P. 2010. Plant immunity: Towards an integrated view of
676 plant-pathogen interactions. Nat. Rev. Genet. 11: 539–548.

677 Dracatos, P.M., Zhang, P., Park, R.F., McIntosh, RA, Wellings, CR. 2016.
678 Complementary resistance genes in wheat selection ‘Avocet R’ confer resistance
679 to stripe rust. Theor. Appl. Genet. 129: 65–76.

680 Engler, C., Youles, M., Gruetzner, R., Ehnert, T.M., Werner, S., Jones, J.D., Patron,
681 N.J., and Marillonnet, S. 2014. A golden gate modular cloning toolbox for plants.
682 ACS Synth Biol. 3: 839-43.

683 Flor, H.H. (1971). Current status of the gene-for-gene concept. Annual Review of
684 Phytopathology, 9, 275–296.

685 Hovmøller, M.S., Walter, S., and Justesen, A.F. 2010. Escalating threat of wheat rusts.
686 Science 329: 369.

687 Hovmøller, M.S., Rodriguez-Algaba, J., Thach, T., and Sørensen, C.K. (2017). "Race
688 typing of *Puccinia striiformis* on wheat," in Wheat rust diseases, methods and
689 protocols. Editor S. Periyannan (N.Y., U.S.A: Springer Protocols Methods in
690 Molecular Biology), 29–40.

691 Hovmøller, M.S., Thach, T., Rodriguez-Algaba, J., Hansen, J.G., Meyer, M., Hodson,
692 D., Nazari, K., Park, R.F., Tam, R., Möller, M., Schwessinger, B., Rathjen, J.P.,
693 Silva, P., Riella, V., and Justesen, A.F. 2025. Long-term surveillance suggests
694 multiple hybridization events by nuclear reassortment and accelerated
695 intercontinental spread of wheat yellow rust. bioRxiv 2025.05.22.655633. doi:
696 10.1101/2025.05.22.655633

697 Jones, J., and Dangl, J. 2006. The plant immune system. Nature 444: 323–329.

698 Jumper, J., Evans, R., Pritzel, A., Green, T., Figurnov, M., Ronneberger, O.,
699 Tunyasuvunakool, K., Bates, R., Žídek, A., Potapenko, A., et al. 2021. Highly
700 accurate protein structure prediction with AlphaFold. Nature, 596: 583–589.

701 Katoh, K, Standley, D.M. 2013. MAFFT multiple sequence alignment software version
702 7: improvements in performance and usability. Mol. Biol. Evol. 30: 772-80.

703 Khan, A., Lloyd, J.P.B., Kidd, B., Lister, R. 2022. Protoplast isolation and transfection
704 in a 96-well plate. protocols.io. doi: 10.17504/protocols.io.yxmvmn1d6g3p/v1

705 Lawrence, G.J., Mayo, G.M.E., and Shepherd, K.W. 1981. Interactions between genes
706 controlling pathogenicity in the flax rust fungus. Phytopathology 71: 12–19.

707 Li, H. 2018. Minimap2: pairwise alignment for nucleotide sequences. Bioinformatics.
708 34: 3094–3100.

709 Livbjerg, M., Rodriguez-Algaba, J., Brown, J.K.M., Sørensen, C.K., Hovmøller, M.,
710 Justesen, A.F. 2025. Genetics of avirulence and interacting inhibitors in *Puccinia*
711 *striiformis f. sp. tritici*. Fungal Genet. Biol. 181: 104037.

712 Lloyd, J.P.B., Ly, F., Gong, P., Pflueger, J., Swain, T., Pflueger, C., Fourie, E., Khan,
713 M.A., Kidd, B.N., and Lister, R. 2022. Synthetic memory circuits for stable cell
714 reprogramming in plants. Nat. Biotechnol. 40: 1862–1872.

715 Love, M.I., Huber, W., and Anders, S. 2014. Moderated estimation of fold change and
716 dispersion for RNA-seq data with DESeq2. Genome Biol. 15: 550.

717 Meile, L., Croll, D., Brunner, P.C., Plissonneau, C., Hartmann, F.E., McDonald, B.A.,
718 and Sánchez-Vallet, A. 2018. A fungal avirulence factor encoded in a highly plastic
719 genomic region triggers partial resistance to septoria tritici blotch. New Phytol.
720 219: 1048-1061.

721 Meng, E.C., Goddard, T.D., Pettersen, E.F., Couch, G.S., Pearson, Z.J., Morris, J.H.,
722 and Ferrin, T.E. 2023. UCSF ChimeraX: Tools for structure building and analysis.
723 Protein Sci. 32: e4792.

724 Miya, A., Albert, P., Shinya, T., Desaki, Y., Ichimura, K, Shirasu, K, Narusaka, Y.,
725 Kawakami, N, Kaku, H, and Shibuya, N. 2007. CERK1, a LysM receptor kinase,
726 is essential for chitin elicitor signaling in Arabidopsis. PNAS.104:19613-8.

727 Nazari, K., and El Amil, R. 2013. First report of resistance of wheat line Avocet '*S*' to
728 stripe rust caused by *Puccinia striiformis* f. sp. *tritici* (*Pst*) in Syria. Plant Dis. 97:
729 996.

730 Oliveira-Garcia, E., Yan, X., Oses-Ruiz, M., de Paula, S., and Talbot, N.J. 2023.
731 Effector-triggered susceptibility by the rice blast fungus *Magnaporthe oryzae*. New
732 Phytol. 24: 1007-1020.

733 Outram, M.A., Chen, J., Broderick, S., Li, Z., Aditya, S., Tasneem, N., Arndell, T.,
734 Blundell, C., Ericsson, D.J., Figueroa, M., Sperschneider, J., Dodds, P.N., and
735 Williams, S.J. 2024. *Avr*Sr27 is a zinc-bound effector with a modular structure
736 important for immune recognition. New Phytol. 243: 314-329.

737 Pereira, E., Baig, D.I., and Schwessinger, B. 2025. Wheat protoplast preparation and
738 transformation in a 96-well plate. protocols.io. doi:
739 10.17504/protocols.io.5qpvod1ndg4o/v1

740 Praz, C.R., Bourras, S., Zeng, F., Sanchez-Martın, J., Menardo, F., Xue, M., Yang, L.,
741 Roffler, S., Boni, R., Herren, G., McNally, K.E., Ben-David, R., Parlange, F.,
742 Oberhaensli, S., Flückiger, S., Schäfer, L.K., Wicker, T., Yu, D., and Keller, B. 2017.
743 *Avr*Pm2 encodes an RNaselike avirulence effector which is conserved in the two
744 different specialized forms of wheat and rye powdery mildew fungus. New Phytol.
745 213: 1301–1314.

746 Ramírez-Zavaleta, C.Y., García-Barrera, L.J., Rodríguez-Verástegui, L.L., Arrieta-
747 Flores, D., and Gregorio-Jorge, J. 2022. An overview of PRR- and NLR-mediated
748 immunities: conserved signaling components across the plant kingdom that
749 communicate both pathways. Int. J. Mol. Sci. 23: 12974.

750 Redkar, A., Jaeger, E., and Doehlemann, G. 2018. Visualization of growth and
751 morphology of fungal hyphae in planta using WGA-AF488 and propidium iodide
752 co-staining. Bio-Protocol. 8: e2942.

753 Rhodes, J., Zipfel, C., Jones, J.D.G., and Ngou, B.P.M. 2022. Concerted actions of
754 PRR- and NLR-mediated immunity. Essays Biochem. 66: 501-511.

755 Salcedo, A., Rutter, W., Wang, S., Akhunova, A., Bolus, S., Chao, S., Anderson, N.,
756 De Soto, M.F., Rouse, M., Szabo, L., Bowden, R.L., Dubcovsky, J., Akhunov, E.

757 2017. Variation in the AvrSr35 gene determines Sr35 resistance against wheat
758 stem rust race Ug99. Science. 358: 1604-1606.

759 Schwessinger, B. (2017). Fundamental wheat stripe rust research in the 21st century.
760 New Phytol. 213: 1625-1631.

761 Schwessinger, B., Sperschneider, J., Cuddy, W.S., Garnica, D.P., Miller, M.E., Taylor,
762 J.M., Dodds, P.N., Figueroa, M., Park, R.F., and Rathjen, J.P. 2018. A near-
763 complete haplotype-phased genome of the dikaryotic wheat stripe rust fungus
764 *Puccinia striiformis* f. sp. *tritici* reveals high interhaplotype diversity. mBio 9:
765 e02275-17

766 Shen, S., Wang, F., Cui, Z. Yuan, S., Meng, L., Liu, D., Ma, L., and Wang, H., 2024.
767 *Puccinia triticina* avirulence protein *AvrLr21* directly interacts with wheat
768 resistance protein *Lr21* to activate wheat immune response. Commun. Biol. 7:
769 1170.

770 Sohn, K.H., Lei, R., Nemri, A., and Jones, J.D. 2007. The downy mildew effector
771 proteins *ATR1* and *ATR13* promote disease susceptibility in *Arabidopsis thaliana*.
772 Plant Cell. 19: 4077-90.

773 Sperschneider, J., and Dodds, P.N. 2022. EffectorP 3.0: Prediction of apoplastic and
774 cytoplasmic effectors in fungi and oomycetes. Mol. Plant Microbe. 35: 146-156.

775 Tam, R., Möller, M., Luo, R., Luo, Z., Jones, A., Periyannan, S., Rathjen, J.P.,
776 Schwessinger, B. 2025. Long-read genomics reveal extensive nuclear-specific
777 evolution and allele-specific expression in a dikaryotic fungus. Genome Res. 11:
778 gr.280359.124.

779 Teufel, F., Almagro Armenteros, J.J., Johansen, A.R., Gíslason, M.H., Pihl, S.I.,
780 Tsirigos, K.D., Winther, O., Brunak, S., von Heijne, G., and Nielsen, H. 2022.

781 SignalP 6.0 predicts all five types of signal peptides using protein language
782 models. Nat. Biotechnol. 40: 1023-1025.

783 Upadhyaya, N.M., Mago, R., Panwar, V., Hewitt, T., Luo, M., Chen, J., Sperschneider,
784 J., Nguyen-Phuc, H., Wang, A., Ortiz, D., Hac, L., Bhatt, D., Li, F., Zhang, J., Ayliffe,
785 M., Figueroa, M., Kanyuka, K., Ellis, J.G., and Dodds, P.N. 2021. Genomics
786 accelerated isolation of a new stem rust avirulence gene-wheat resistance gene
787 pair. Nat Plants. 7: 1220-1228.

788 Wang, J., Chen, T., Tang, Y., Zhang, S., Xu, M., Liu, M., Zhang, J., Loake, G.J., and
789 Jiang, J. 2023. The Biological Roles of *Puccinia striiformis* f. sp. *tritici* Effectors
790 during Infection of Wheat. Biomolecules. 13: 889.

791 Wang, J., Xu, Y., Peng, Y., Wang, Y., Kang, Z., and Zhao, J. 2024. A fully haplotype-
792 resolved and nearly gap-free genome assembly of wheat stripe rust fungus. Sci.
793 Data. 11: 508.

794 Wilson, S., Dagvadorj, B., Tam, R., Schwessinger, B. (n.d.). Wheat protoplast
795 preparation and transformation (Version 1). protocols.io. doi:
796 10.17504/protocols.io.q26g7r3zkvwz/v1

797 Wilson, S., Dagvadorj, B., Tam, R., Murphy, L., Schulz-Kroenert, S., Heng, N., Crean,
798 E., Greenwood, J., Rathjen, J.P., and Schwessinger, B. 2024. Multiplexed effector
799 screening for recognition by endogenous resistance genes using positive defense
800 reporters in wheat protoplasts. New Phytol. 241: 2621-2636.

801 Win, J., Chaparro-Garcia, A., Belhaj, K., Saunders, D.G., Yoshida, K., Dong, S.,
802 Schornack, S., Zipfel, C., Robatzek, S., Hogenhout, S.A., and Kamoun, S. 2012.
803 Effector biology of plant-associated organisms: concepts and perspectives. Cold
804 Spring Har. Symp. Quant. Biol. 77: 235–247.

805 Wu, C.H., and Derevnina, L. 2023. The battle within: How pathogen effectors suppress
806 NLR-mediated immunity. Curr. Opin. Plant Biol. 74: 102396.

807 Xia, C., Lei, Y., Wang, M., Chen, W., and Chen, X. 2020. An avirulence gene cluster in
808 the wheat stripe rust pathogen (*Puccinia striiformis* f. sp. *tritici*) identified through
809 genetic mapping and whole-genome sequencing of a sexual population. mSphere
810 5: 10.1128/msphere.00128-20.

811 Yu, D.S., Outram, M.A., Smith, A., McCombe, C.L., Khambalkar, P.B., Rima, S.A., Sun,
812 X., Ma, L., Ericsson, D.J., Jones, D.A., and Williams, S.J. 2024. The structural
813 repertoire of *Fusarium oxysporum* f. sp. *lycopersici* effectors revealed by
814 experimental and computational studies. Elife.12: RP89280.

815 Zhang, X., Farah, N., Rolston, L., Ericsson, D.J., Catanzariti, A.M., Bernoux, M., Ve,
816 T., Bendak, K., Chen, C., Mackay, J.P., Lawrence, G.J., Hardham, A., Ellis, J.G.,
817 Williams, S.J., Dodds, P.N., Jones, D.A., and Kobe, B. 2018. Crystal structure of
818 the *Melampsora lini* effector AvrP reveals insights into a possible nuclear function
819 and recognition by the flax disease resistance protein. P. Mol. Plant Pathol. 19:
820 1196-1209.

821 Zheng, P., Liu, M., Pang, L., Sun, R., Yao, M., Wang, X., Kang, Z., and Liu, J. 2023.
822 Stripe rust effector *Pst*21674 compromises wheat resistance by targeting
823 transcription factor TaASR3. Plant Physiol. 193: 2806-2824.

824 Zhong, Z., Marcel, T.C., Hartmann, F.E., Ma, X., Plissonneau, C., Zala, M., Ducasse,
825 A., Confais, J., Compain, J., Lapalu, N., Amselem, J., McDonald, B.A., Croll, D.,
826 Palma-Guerrero, J. 2017. A small secreted protein in *Zymoseptoria tritici* is
827 responsible for avirulence on wheat cultivars carrying the *Stb6* resistance gene.
828 New Phytol. 214, 619-631.

829 ## Figures

830 **Figure 1 – *pDefense* D14 promoter activation triggered by *AvrPstB48* in Avocet *Yr5* and Avocet**
831 ***S* protoplasts**. Dual luciferase-based reporter assays were performed using wheat protoplasts from
832 wheat cultivars Avocet *Yr5* **a)** and Avocet *S* **b)** to assess defence signalling. The x-axis shows the
833 plasmid combinations tested, including candidate effectors *Pst104E137_008104* (#47),
834 *Pst104E137_010232* (*AvrPstB48*), and *Pst104E137_024713* (#49), along with the positive control pair
835 *AvrSr50/Sr50*. The y-axis represents normalised luminescence values, measured as the ratio of
836 luciferase activity driven by the D14 promoter to the internal control UBI-pRed. *AvrPstB48* triggered a
837 significant increase in reporter activity, indicating activation of defence responses. Statistical differences
838 were analysed using one-way ANOVA followed by Tukey's Honestly Significant Difference (HSD) test;
839 Conditions with different letters are significantly different from each other ($p < 0.05$).

840

841 **Figure 2 – Genomic, evolutionary, and structural characterisation of the candidate effector gene**
842 ***AvrPstB48* and its paralogs. a)** Genomic organisation and synteny of *AvrPstB48*
843 (*Pst104E137_010232*) and its paralogs (P1: *Pst104E137_025766*; P2: *Pst104E137_025767*; P3:
844 *Pst104E137_010231*; P4: *Pst104E137_010234*) across homologous regions of Chromosomes 10A and
845 10B, with genes shown as red or blue arrows, respectively. Grey-shaded blocks and contained numbers
846 represent pairwise nucleotide sequence identity (%) between all paralogs. **b)** Multiple sequence
847 alignment of *AvrPstB48* and its paralogs, showing conservation at the amino acid level. Identical or
848 similar residues are highlighted using the Clustal X colour scheme, which assigns colours based on
849 amino acid conservation and properties. Conserved motifs are evident across the sequences. Dashes
850 indicate gaps in the alignment. Pink shading marks the predicted N-terminal signal peptide; orange bars
851 denote predicted α-helical segments; red arrows denote predicted β-strands mapped from the
852 AlphaFold3 structural model onto the multiple-sequence alignment of *AvrPstB48* and its paralogs (*P1,*
853 *P2/P4, P3*). **c)** Superposition of AlphaFold3 models for *AvrPstB48* and its paralogs. Global backbone
854 similarity is high (pairwise RMSD ~0.5–1.5 Å), with most divergence at the C-terminal helical region.
855 Predicted model confidences (pTM ~0.50–0.57) indicate hypothesis-generating structures rather than
856 definitive models. Colour key: *AvrPstB48* (green), *P1* (orange), *P2/4* (pink), *P3* (light blue). The N-
857 terminus are represented by green arrows and the C-terminus by red arrows, and includes *AvrPstB48*

858 (C48) paralog (PX) labelling. **d)** Expression profile of *AvrPstB48* and its paralogs in ungerminated
859 urediniospores (UG) and infected wheat leaves at 4, 6, 8, 10 and 12 days post-infection (dpi) *in planta*.
860 RNA-seq abundance was normalised using DESeq's median of ratio method and plotted as box plots
861 with four biological replicates. Analysis of variance (ANOVA) was performed using a two-way ANOVA
862 with sampling condition (UG, 4, 6, 8, 10 and 12 dpi) and effector identity (*AvrPstB48, P1, P2, P3* and
863 *P4*) as fixed factors, followed by post hoc Tukey's Honestly Significant Difference (HSD) test. Sampling
864 condition –effector combinations marked with distinct letters indicate that they are significantly different
865 ($p < 0.05$) according to Tukey's post hoc multiple-comparisons test. Boxes represent the interquartile
866 range with the horizontal line inside the box indicating the median.

867

868 **Figure 3 – Differential activation of defence reporters by *AvrPstB48* reveals genotype-dependent**
869 **recognition.** Normalised luminescence signals from dual luciferase-based reporter assays using three
870 promoter constructs (pD14, pD2, pD15) and UBI-pRedf in **a)** Avocet S and **b)** Morocco. *AvrSr50* and
871 *AvrSr50:Sr50* were used as negative and positive controls, respectively. One-way analysis of variance
872 (ANOVA) followed by Tukey's Honestly Significant Difference (HSD) test was used to compare
873 treatments. Conditions with different letters are significantly different from each other ($p < 0.05$).

874

875 **Figure 4 – Differential activation of defence reporters by *AvrPstB48* paralogs reveals genotype-**
876 **dependent recognition.** Normalised luminescence signals from dual luciferase-based reporter assays
877 using the pD14 promoter construct and UBI-pRedf in **a)** Avocet S, **b)** Morocco and **c)** Co-expression of
878 *AvrPstB48* and *AvrPstB48_P3* (#48:P3) and *AvrPstB48* and Empty Vector (#48:ev) at a 1:1 plasmid
879 ratio in Avocet S. *AvrSr50* and *AvrSr50:Sr50* were included as negative and positive controls. One-way
880 analysis of variance (ANOVA) followed by Tukey's Honestly Significant Difference (HSD) test was used
881 to compare treatments. Conditions with different letters are significantly different from each other ($p <$
882 0.05).

883

884 **Figure 5 – A single amino acid (D134) is necessary but not sufficient for recognition of *AvrPstB48***
885 **and its paralog *AvrPstB48_P3*. a)** Predicted structures of *AvrPstB48* and *AvrPstB48*_P3 were

886 generated using AlphaFold3. The surface-exposed amino acid position 134 is highlighted where
887 *AvrPstB48*, *P1*, and *P2/P4* encode an aspartic acid (D), while P3 encodes a glycine (G). **b)** Normalised
888 luminescence signals from dual luciferase-based reporter assays using the pD14 promoter and UBI-
889 pRedf. One-way analysis of variance (ANOVA) followed by the Tukey Honestly Significant Difference
890 (HSD) test was used to compare the treatments. Conditions with different letters are significantly
891 different from each other ($p < 0.05$).
892

893 **Figure 6. The susceptible wheat cultivar Avocet S displays a delayed infection time course to**
894 ***Pst*104E137A- when compared to Morocco. a)** Leaf phenotypes at 8 and 10 days post-infection (dpi).
895 **b)** Representative confocal micrographs showing the extent of infection inside the leaves at 8 and 10
896 dpi. Magenta corresponds to propidium iodide-stained cell walls, and green to fungal structures stained
897 with wheat germ agglutinin. Bars = 200 µm. **c)** Representative confocal micrographs showing callose
898 deposition (cyan) associated with infectious hyphae (magenta). Bars = 25 µm. **d)** Infection progression
899 and **e)** callose deposition through time in infected leaves. Asterisks denote significant differences
900 according to Welch's t-test at *p*-value < 0.01 (**) and *p*-value < 0.001 (***).

901

902 ## Supplementary Figures

903 **Figure S1 - Differential activation of defence reporters by *AvrPstB48* reveals genotype-**
904 **dependent recognition.** Normalised luminescence signals from dual luciferase-based reporter assays
905 using three promoter constructs (pD14, pD2, pD15) and UBI-pRedf in **a)** Triticum spelta *Yr5*, **b)** Gabo
906 and **c)** Chinese 166. AvrSr50 and AvrSr50:Sr50 were used as negative and positive controls,
907 respectively. One-way analysis of variance (ANOVA) followed by Tukey's Honestly Significant
908 Difference (HSD) test was used to compare treatments. Conditions with different letters are significantly
909 different from each other ($p < 0.05$).

910

911 **Figure S2 - Differential activation of defence reporters by *AvrPstB48* paralogs reveals genotype-**
912 **dependent recognition.** Normalised luminescence signals from dual luciferase-based reporter assays
913 using the pD14 promoter construct and UBI-pRedf in **a)** *Triticum spelta Yr5*, **b)** Gabo and **c)** Chinese
914 166. AvrSr50 and AvrSr50:Sr50 were included as negative and positive controls, respectively. One-way
915 analysis of variance (ANOVA) followed by Tukey's Honestly Significant Difference (HSD) test was used
916 to compare treatments. Conditions with different letters are significantly different from each other ($p <$
917 0.05).

918

919 **Figure S3 – Endpoint RT-PCR confirmation of transgene expression in wheat protoplasts.** Total
920 RNA from transfected protoplasts was DNase-treated and reverse-transcribed. Gene-specific primers
921 amplified *AvrPstB48*, *AvrPstB48_P3*, and wheat 18S rRNA (Ta 18s; loading control). Five microlitres of
922 each amplicon were resolved on a 1% agarose gel and visualised under UV. M, 1 kb Plus DNA Ladder
923 (NEB #N3200).

924

925 **Figure S4** – **Infection types of selected wheat cultivars inoculated with Pst104E137A–.** Infection
926 types (IT) on a 0-9 scale on the wheat cultivars *Triticum spelta Yr5*, Avocet *S*, Chinese 166, Morocco
927 and Gabo at 12 days post-infection (DPI). 0: no visible disease symptoms (immune), 1: minor chlorotic
928 and necrotic flecks, 2: chlorotic and necrotic flecks without sporulation, 3–4: chlorotic and necrotic areas
929 with limited sporulation, 5–6: chlorotic and necrotic areas with moderate sporulation, 7: abundant

930 sporulation with moderate chlorosis, 8–9: abundant and dense sporulation without notable chlorosis
931 and necrosis.

932

933 ## Supplementary Tables

934 **Table S1 - Comparative sequence alignment and AlphaFold modelling metrics for AvrPstB48 and**
935 **paralogs *(P1, P2/P4, P3*).** The AlphaFold metrics include ipTM (interface predicted TM-score) and
936 pTM (predicted TM-score), which estimate confidence in the predicted structures and inter-domain
937 orientations, with higher values indicating greater reliability. The “Zn” column indicates whether zinc
938 ions were included during modelling, as zinc can stabilise cysteine-rich proteins and influence predicted
939 folding.

940

941 **Table S2 – Primers used for Avr insert verification and RT–PCR.** Primer names, functions and
942 sequences used to confirm the presence of Avr inserts (DB34, DB35) after cloning and for cDNA
943 amplification of AvrPstB48, AvrPstB48_P3 and the wheat reference gene Ta18S in RT–PCR.

944

945 **Table S3 - List of plasmids.**

946

947 **Table S4 - List of Avirulence (Avr) screening in wheat protoplasts of various differential wheat**
948 **lines to *Puccinia striiformis* f. sp. *tritici* (*Pst*) Pst104E137A-infection in a protoplast-based**
949 **defence reporter assay.**

950

951 **Table S5 – Resume of promoter activation triggered by *AvrPstB48* and Infection types (IT) on a**
952 **0-9 scale for the isolate 104E137A- inoculated in different cultivars.** Response of various
953 differential wheat lines to *Puccinia striiformis* f. sp. *tritici* (*Pst*) *Pst*104E137A-infection and the induction
954 of *AvrPstB48* in a protoplast-based defence reporter assay. "*Pst*-resistant gene" refers to the known Yr
955 gene(s) present in each line. "*AvrPstB48* induction" indicates whether candidate *AvrPstB48* triggered a

defence response (+) or not (-) in the protoplast assay. "*Pst* infection *outcomes*" represents the infection types (IT) on a 0-9 scale on the wheat cultivars at 12 days post-infection (DPI). 0: no visible disease symptoms (immune), 1: minor chlorotic and necrotic flecks, 2: chlorotic and necrotic flecks without sporulation, 3–4: chlorotic and necrotic areas with limited sporulation, 5–6: chlorotic and necrotic areas with moderate sporulation, 7: abundant sporulation with moderate chlorosis, 8–9: abundant and dense sporulation without notable chlorosis and necrosis.

Figures

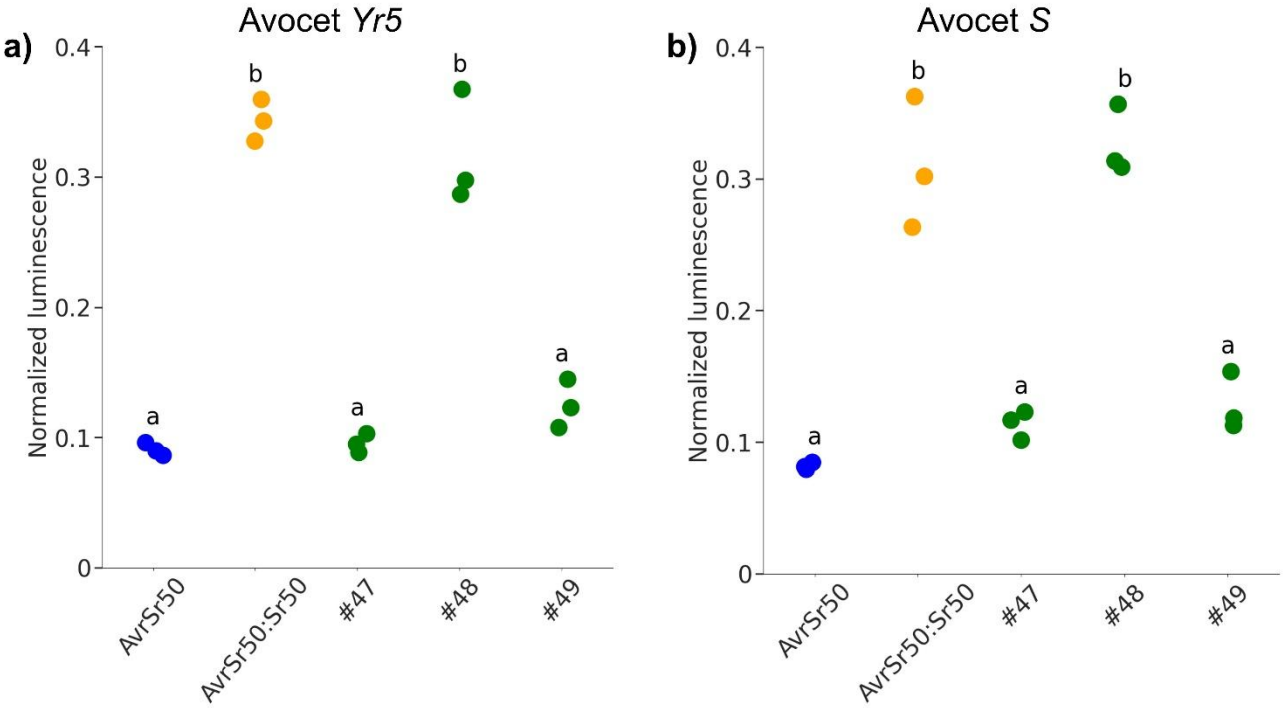

Figure 1 – *pDefense* D14 promoter activation triggered by *AvrPstB48* in Avocet *Yr5* and Avocet S protoplasts. Dual luciferase-based reporter assays were performed using wheat protoplasts from wheat cultivars Avocet *Yr5* **a)** and Avocet *S* **b)** to assess defence signalling. The x-axis shows the plasmid combinations tested, including candidate effectors *Pst104E137_008104* (#47), *Pst104E137_010232* (*AvrPstB48*), and *Pst104E137_024713* (#49), along with the positive control pair *AvrSr50/Sr50*. The y-axis represents normalised luminescence values, measured as the ratio of luciferase activity driven by the D14 promoter to the internal control UBI-pRed. *AvrPstB48* triggered a significant increase in reporter activity, indicating activation of defence responses. Statistical differences were analysed using one-way ANOVA followed by Tukey's Honestly Significant Difference (HSD) test; Conditions with different letters are significantly different from each other ($p < 0.05$).

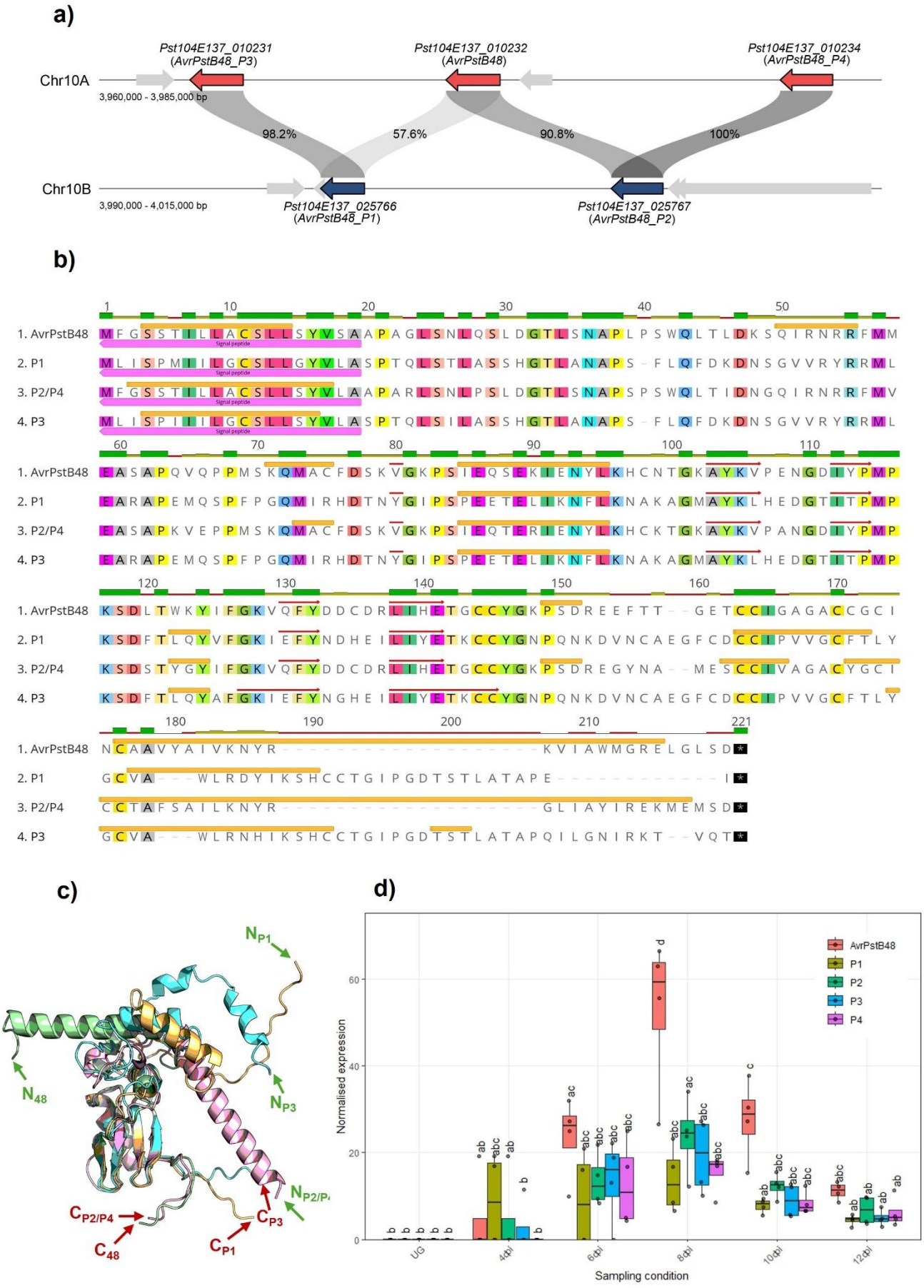
a)
Pst104E137_010231
(AvrPstB48_P3)
Pst104E137_010232
(AvrPstB48)
Pst104E137_010234
(AvrPstB48_P4)
Chr10A
3,960,000 - 3,985,000 bp
98.2%
57.6%
90.8%
100%
Chr10B
3,990,000 - 4,015,000 bp
Pst104E137_025766
(AvrPstB48_P1)
Pst104E137_025767
(AvrPstB48_P2)
b)
1. AvrPstB48
2. P1
3. P2/P4
4. P3
Signal peptide
c)
N_P1
N_48
N_P3
N_P2/P4
C_P2/P4
C_48
C_P1
C_P3
d)
AvrPstB48
P1
P2
P3
P4
Normalised expression
Sampling condition
UG
4dpi
6dpi
8dpi
10dpi
12dpi

Figure 2 – Genomic, evolutionary, and structural characterisation of the candidate effector gene *AvrPstB48* and its paralogs. a) Genomic organisation and synteny of *AvrPstB48* (*Pst104E137_010232*) and its paralogs (P1: *Pst104E137_025766*; P2: *Pst104E137_025767*; P3: *Pst104E137_010231*; P4: *Pst104E137_010234*) across homologous regions of Chromosomes 10A and 10B, with genes shown as red or blue arrows, respectively. Grey-shaded blocks and contained numbers represent pairwise nucleotide sequence identity (%) between all paralogs. **b)** Multiple sequence alignment of *AvrPstB48* and its paralogs, showing conservation at the amino acid level. Identical or similar residues are highlighted using the Clustal X colour scheme, which assigns colours based on amino acid conservation and properties. Conserved motifs are evident across the sequences. Dashes indicate gaps in the alignment. Pink shading marks the predicted N-terminal signal peptide; orange bars denote predicted α-helical segments; red arrows denote predicted β-strands mapped from the AlphaFold3 structural model onto the multiple-sequence alignment of *AvrPstB48* and its paralogs (*P1, P2/P4, P3*). **c)** Superposition of AlphaFold3 models for *AvrPstB48* and its paralogs. Global backbone similarity is high (pairwise RMSD ~0.5–1.5 Å), with most divergence at the C-terminal helical region. Predicted model confidences (pTM ~0.50–0.57) indicate hypothesis-generating structures rather than definitive models. Colour key: *AvrPstB48* (green), *P1* (orange), *P2/4* (pink), *P3* (light blue). The N-terminus are represented by green arrows and the C-terminus by red arrows, and includes *AvrPstB48* (C48) paralog (PX) labelling. **d)** Expression profile of *AvrPstB48* and its paralogs in ungerminated urediniospores (UG) and infected wheat leaves at 4, 6, 8, 10 and 12 days post-infection (dpi) *in planta*. RNA-seq abundance was normalised using DESeq's median of ratio method and plotted as box plots with four biological replicates. Analysis of variance (ANOVA) was performed using a two-way ANOVA with sampling condition (UG, 4, 6, 8, 10 and 12 dpi) and effector identity (*AvrPstB48, P1, P2, P3* and *P4*) as fixed factors, followed by post hoc Tukey's Honestly Significant Difference (HSD) test. Sampling condition –effector combinations marked with distinct letters indicate that they are significantly different ($p < 0.05$) according to Tukey's post hoc multiple-comparisons test. Boxes represent the interquartile range with the horizontal line inside the box indicating the median.

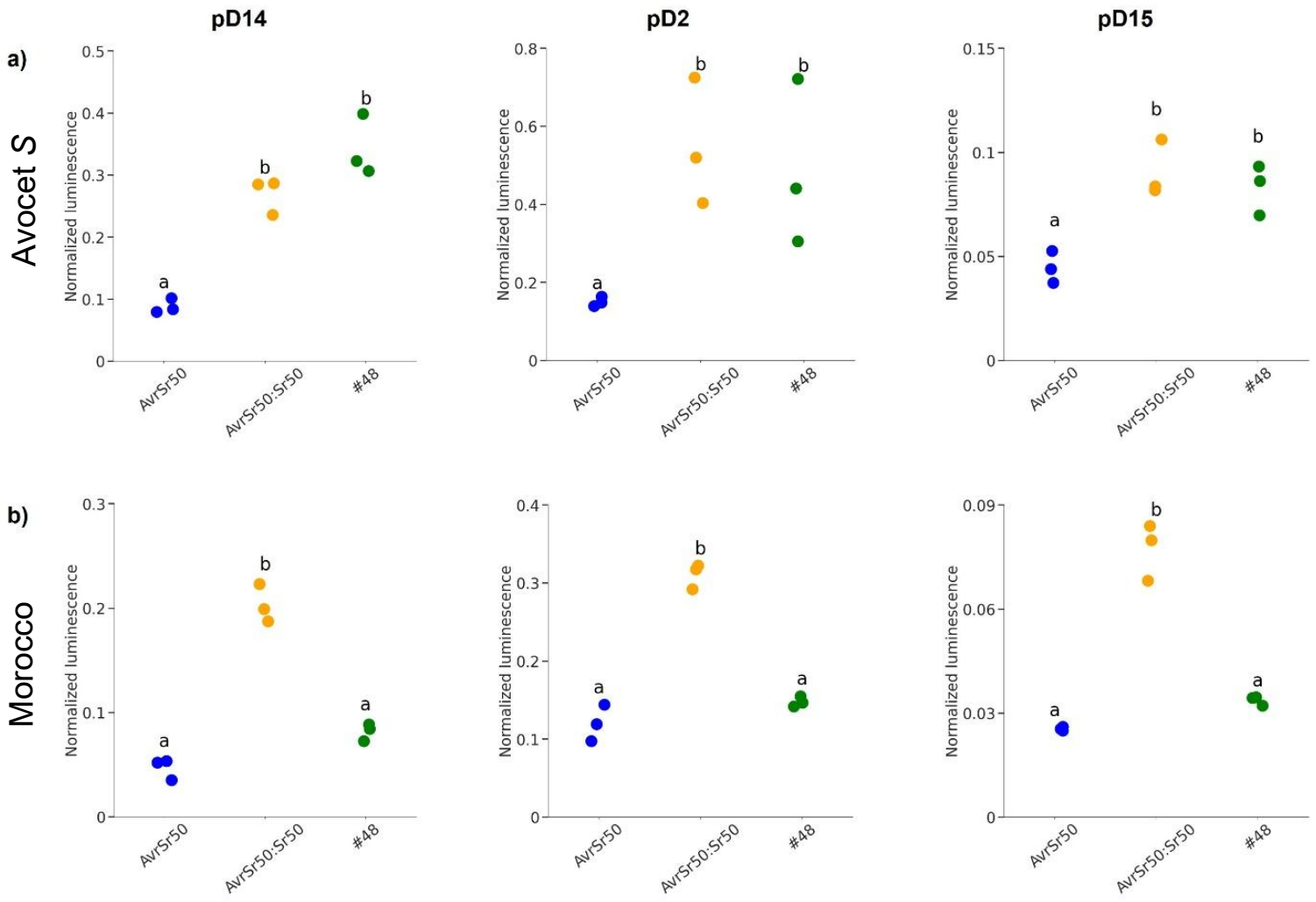

Figure 3 – Differential activation of defence reporters by *AvrPstB48* reveals genotype-dependent recognition. Normalised luminescence signals from dual luciferase-based reporter assays using three promoter constructs (pD14, pD2, pD15) and UBI-pRedf in **a)** Avocet S and **b)** Morocco. *AvrSr50* and *AvrSr50:Sr50* were used as negative and positive controls, respectively. One-way analysis of variance (ANOVA) followed by Tukey's Honestly Significant Difference (HSD) test was used to compare treatments. Conditions with different letters are significantly different from each other ($p < 0.05$).

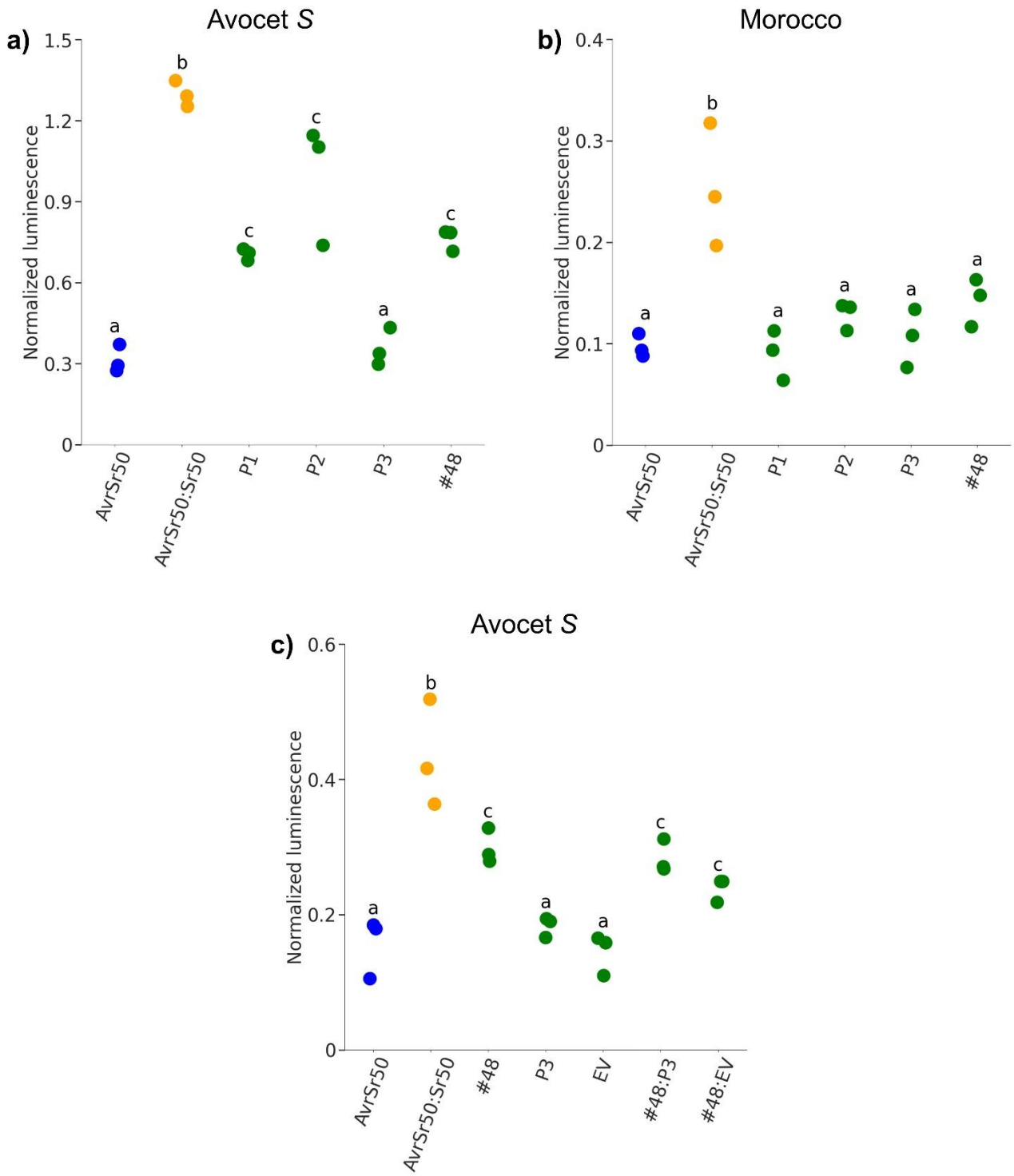

Figure 4 – Differential activation of defence reporters by *AvrPstB48* paralogs reveals genotype-dependent recognition. Normalised luminescence signals from dual luciferase-based reporter assays using the pD14 promoter construct and UBI-pRedf in **a)** Avocet S, **b)** Morocco and **c)** Co-expression of *AvrPstB48* and *AvrPstB48_P3* (#48:P3) and *AvrPstB48* and Empty Vector (#48:ev) at a 1:1 plasmid ratio in Avocet S. *AvrSr50* and *AvrSr50:Sr50* were included as negative and positive controls. One-way

analysis of variance (ANOVA) followed by Tukey's Honestly Significant Difference (HSD) test was used to compare treatments. Conditions with different letters are significantly different from each other ($p < 0.05$).

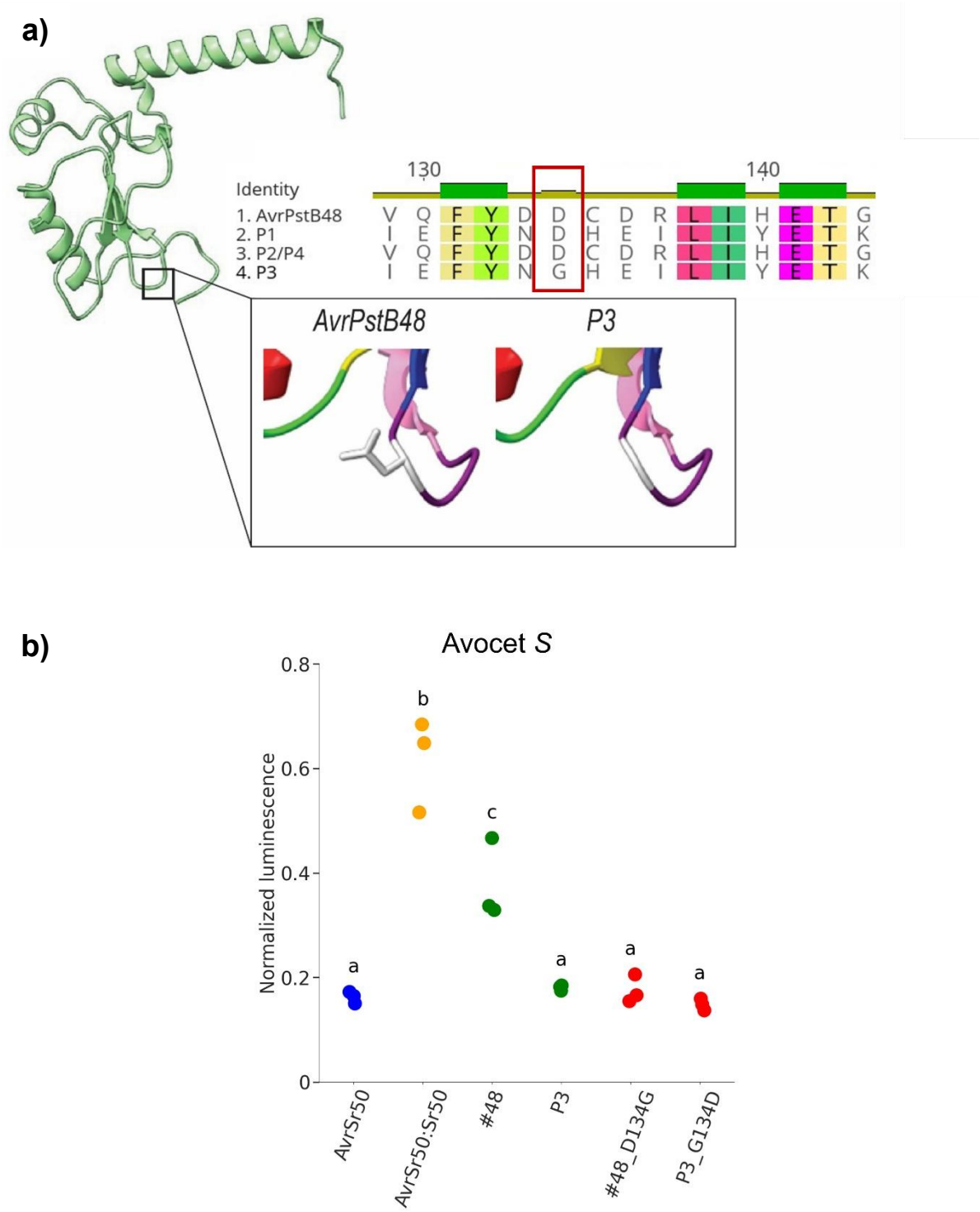

Figure 5 – A single amino acid (D134) is necessary but not sufficient for recognition of *AvrPstB48* and its paralog *AvrPstB48_P3*. a) Predicted structures of *AvrPstB48* and *AvrPstB48*_P3 were generated using AlphaFold3. The surface-exposed amino acid position 134 is highlighted where *AvrPstB48*, *P1*, and *P2/P4* encode an aspartic acid (D), while P3 encodes a glycine (G). **b)** Normalised luminescence signals from dual luciferase-based reporter assays using the pD14 promoter and UBI-

pRedf. One-way analysis of variance (ANOVA) followed by the Tukey Honestly Significant Difference (HSD) test was used to compare the treatments. Conditions with different letters are significantly different from each other ($p < 0.05$).

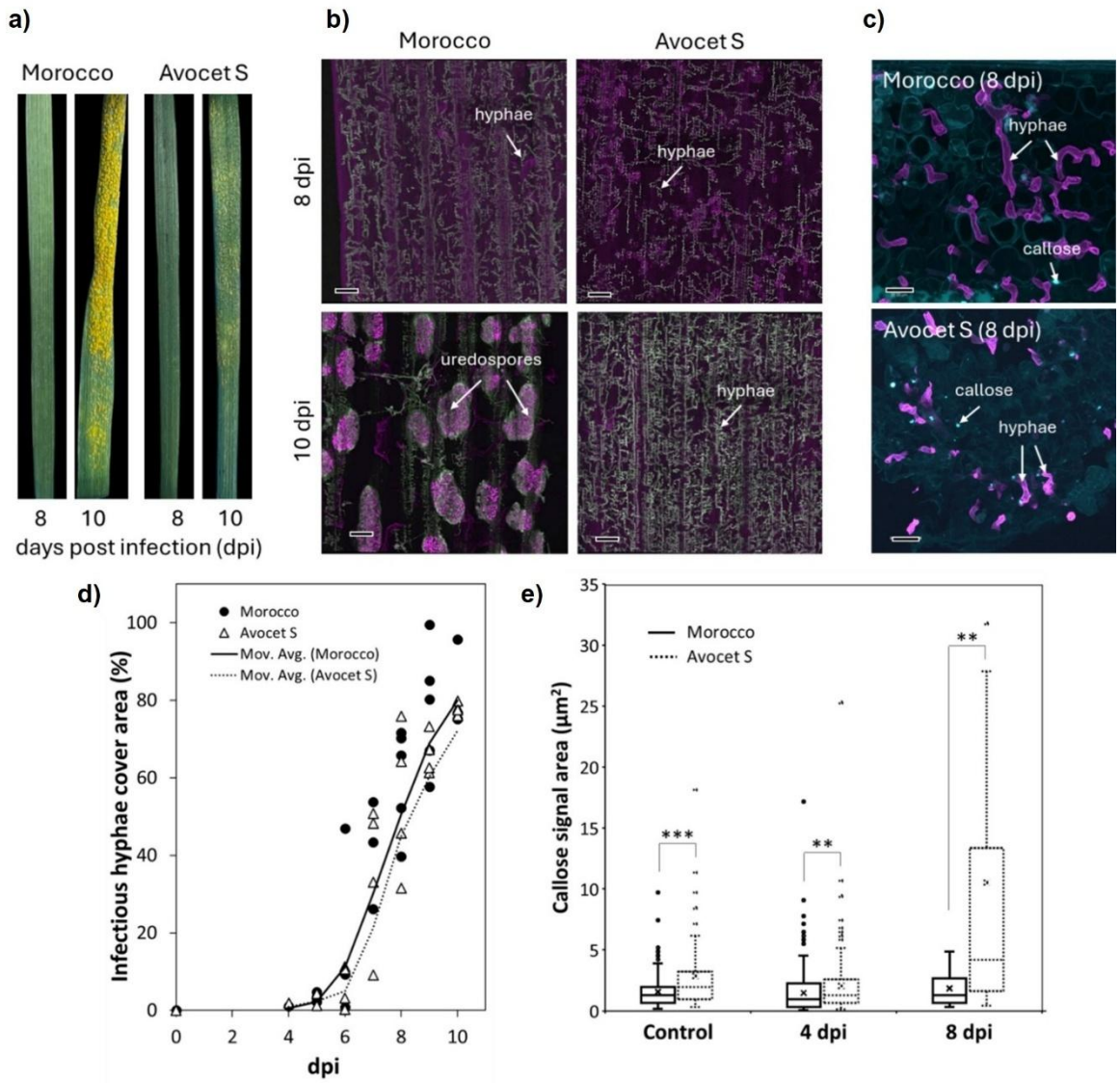

Figure 6. The susceptible wheat cultivar Avocet S displays a delayed infection time course to *Pst*104E137A- when compared to Morocco. a) Leaf phenotypes at 8 and 10 days post-infection (dpi). **b)** Representative confocal micrographs showing the extent of infection inside the leaves at 8 and 10 dpi. Magenta corresponds to propidium iodide-stained cell walls, and green to fungal structures stained with wheat germ agglutinin. Bars = 200 µm. **c)** Representative confocal micrographs showing callose deposition (cyan) associated with infectious hyphae (magenta). Bars = 25 µm. **d)** Infection progression and **e)** callose deposition through time in infected leaves. Asterisks denote significant differences according to Welch's t-test at p-value < 0.01 (**) and p-value < 0.001 (***).

Supplementary Figures

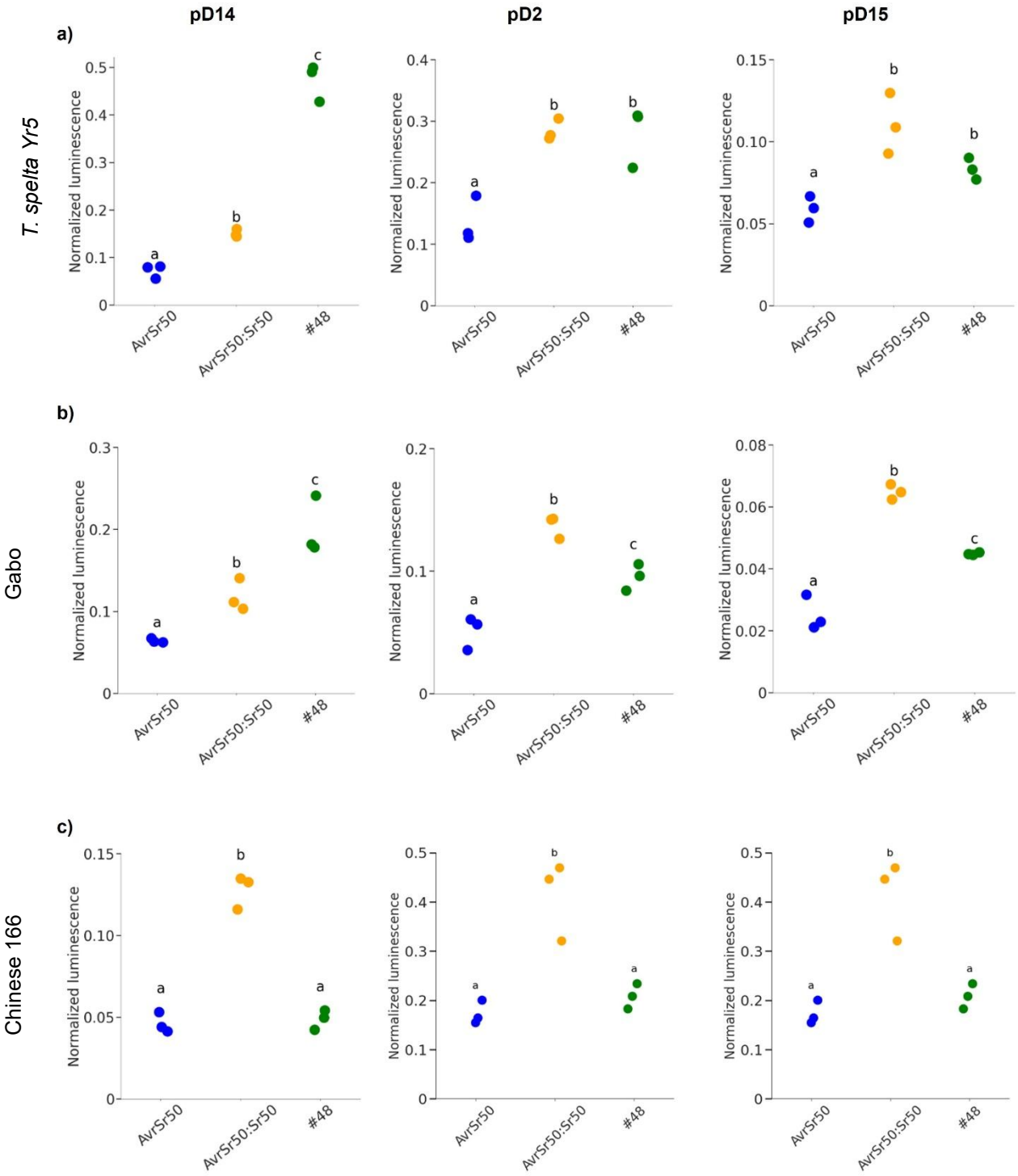

Figure S1 - Differential activation of defence reporters by *AvrPstB48* reveals genotype-dependent recognition. Normalised luminescence signals from dual luciferase-based reporter assays using three promoter constructs (pD14, pD2, pD15) and UBI-pRedf in **a)** Triticum spelta *Yr5*, **b)** Gabo and **c)** Chinese 166. AvrSr50 and AvrSr50:Sr50 were used as negative and positive controls,

respectively. One-way analysis of variance (ANOVA) followed by Tukey's Honestly Significant Difference (HSD) test was used to compare treatments. Conditions with different letters are significantly different from each other ($p < 0.05$).

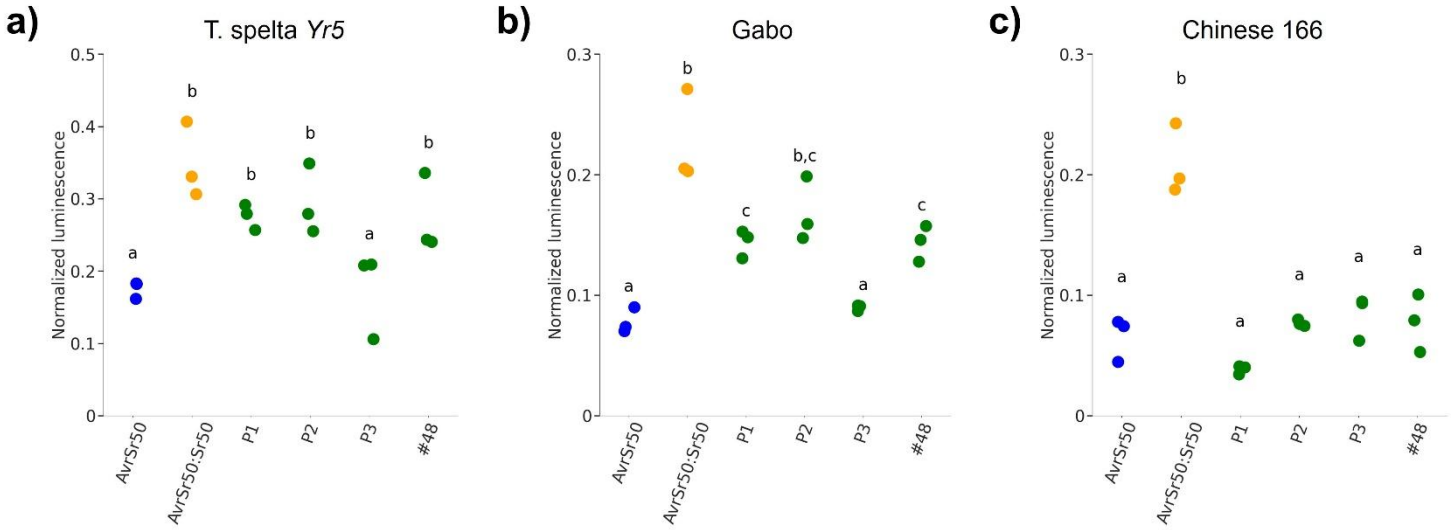

Figure S2 - Differential activation of defence reporters by *AvrPstB48* paralogs reveals genotype-dependent recognition. Normalised luminescence signals from dual luciferase-based reporter assays using the pD14 promoter construct and UBI-pRedf in **a)** *Triticum spelta Yr5*, **b)** Gabo and **c)** Chinese 166. AvrSr50 and AvrSr50:Sr50 were included as negative and positive controls, respectively. One-way analysis of variance (ANOVA) followed by Tukey's Honestly Significant Difference (HSD) test was used to compare treatments. Conditions with different letters are significantly different from each other ($p < 0.05$).

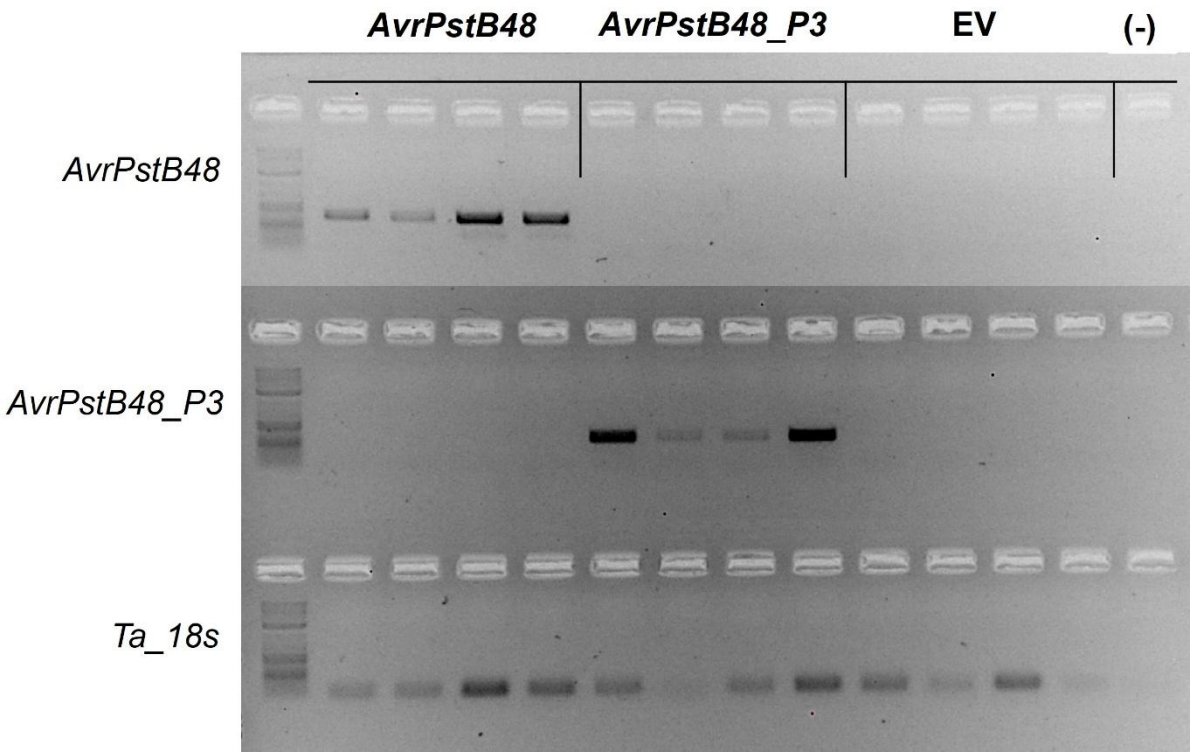

Figure S3 – Endpoint RT-PCR confirmation of transgene expression in wheat protoplasts. Total RNA from transfected protoplasts was DNase-treated and reverse-transcribed. Gene-specific primers amplified *AvrPstB48*, *AvrPstB48_P3*, and wheat 18S rRNA (Ta 18s; loading control). Five microlitres of each amplicon were resolved on a 1% agarose gel and visualised under UV. M, 1 kb Plus DNA Ladder (NEB #N3200).

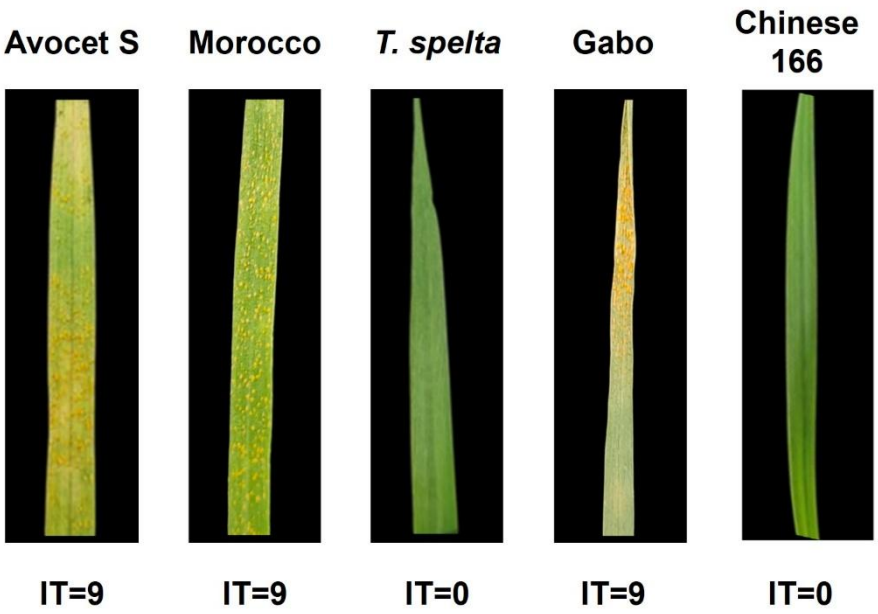

Figure S4 – **Infection types of selected wheat cultivars inoculated with Pst104E137A–.** Infection types (IT) on a 0-9 scale on the wheat cultivars *Triticum spelta Yr5*, Avocet *S*, Chinese 166, Morocco and Gabo at 12 days post-infection (DPI). 0: no visible disease symptoms (immune), 1: minor chlorotic and necrotic flecks, 2: chlorotic and necrotic flecks without sporulation, 3–4: chlorotic and necrotic areas with limited sporulation, 5–6: chlorotic and necrotic areas with moderate sporulation, 7: abundant sporulation with moderate chlorosis, 8–9: abundant and dense sporulation without notable chlorosis and necrosis.